Journal Pre-proofs

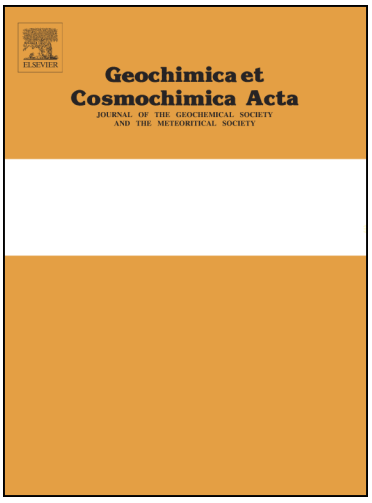

Estimating ancient seawater isotope compositions and global ocean redox conditions by coupling the molybdenum and uranium isotope systems of euxinic organic-rich mudrocks

Xinze Lu, Tais W. Dahl, Wang Zheng, Su Wang, Brian Kendall

PII: S0016-7037(20)30549-4
DOI: https://doi.org/10.1016/j.gca.2020.08.032
Reference: GCA 11904

To appear in: *Geochimica et Cosmochimica Acta*

Received Date: 11 February 2020
Accepted Date: 29 August 2020

Please cite this article as: Lu, X., Dahl, T.W., Zheng, W., Wang, S., Kendall, B., Estimating ancient seawater isotope compositions and global ocean redox conditions by coupling the molybdenum and uranium isotope systems of euxinic organic-rich mudrocks, *Geochimica et Cosmochimica Acta* (2020), doi: https://doi.org/10.1016/j.gca.2020.08.032

Estimating ancient seawater isotope compositions and global ocean redox conditions by coupling the molybdenum and uranium isotope systems of euxinic organic-rich mudrocks

Xinze Lyu[1, *], Tais W. Dahl[2], Wang Zheng[3], Su Wang[1], Brian Kendall[1]

[1]Department of Earth & Environmental Sciences, University of Waterloo, Waterloo, ON, Canada

[2]GLOBE Institute, University of Copenhagen, Copenhagen K, Denmark

[3]Institute of Surface-Earth System Science, Tianjin University Tianjin, China

Re-submitted to *Geochimica et Cosmochimica Acta*

August 2020

* Correspondence to: xlv@uwaterloo.ca

Abstract

The sedimentary Mo and U isotope systems have been commonly used as novel global ocean redox tracers due to their long oceanic residence times and redox-sensitive behavior. However, local sedimentary environments and global ocean redox conditions both influence the Mo and U isotope compositions of euxinic organic-rich mudrocks (ORM). Here, we further develop the coupled use of Mo and U isotope data from euxinic ORM to more robustly infer coeval global ocean redox conditions. We measured $\delta^{238}U$ from eight late Neoproterozoic to middle Paleozoic ORM units that have previously reported Mo isotope and Fe speciation data. Integration of our new data with previously published Proterozoic and Phanerozoic Mo and U isotope data reveals that there is no overall correlation between the Mo and U isotope compositions of euxinic ORM. This observation confirms that the extent to which local versus global environments influenced the preserved Mo and U isotope compositions in ORM was variable. Individual ORM units can have negative, positive, or no correlation between $\delta^{98}Mo$ and $\delta^{238}U$. A negative correlation between $\delta^{98}Mo$ and $\delta^{238}U$ in the Upper Devonian Kettle Point Formation is similar to the observations from modern euxinic basins, reflecting a major control on the Mo-U isotope systematics by changes in the local depositional environment, such as bottom-water sulfide concentrations. A positive correlation between $\delta^{98}Mo$ and $\delta^{238}U$ observed in the Upper Ordovician Fjäcka Shale is best explained by changes in global ocean redox conditions that simultaneously shifted the Mo and U isotope compositions of the global seawater and the Fjäcka Shale ORMs in the same direction. No correlations between $\delta^{98}Mo$ and $\delta^{238}U$ for euxinic ORM may be caused by specific local depositional changes, a lack of or a combination of local and global environmental changes, and/or is an artifact of limited data. For example, a vertical trend (variable $\delta^{98}Mo$ but similar $\delta^{238}U$) is shown by most samples

from Member IV of the Ediacaran Doushantuo Formation, implying a strong influence on the Mo isotope data by an Fe-Mn particulate shuttle. A horizontal trend (similar $\delta^{98}Mo$ but variable $\delta^{238}U$) is observed from the Paleoproterozoic Zaonega Formation, implying that relatively constant bottom water sulfide concentrations caused similar magnitudes of Mo isotope fractionations whereas other factors (e.g., U reduction pathways, aqueous U species, productivity) were responsible for variable U isotope fractionations. Relatively constant elemental concentrations and isotope compositions from the Tanezzuft Formation are indicative of stable conditions at local and global scales. We further propose a method to estimate the coeval seawater Mo and U isotope compositions based on a coupled Mo-U isotope mass balance model and the observations from modern euxinic basins. The coupled Mo-U isotope data from euxinic ORMs provide more insights on the local and global environmental controls on the preservation of both isotope systems than previously realized. Our study highlights the importance of examining the local depositional environment and using large datasets of coupled Mo-U isotope compositions from euxinic ORM intervals to reconstruct paleocean redox conditions.

Keywords: depositional environment, paleoredox proxy, mass balance model

1. INTRODUCTION

Changes in Earth's atmosphere-ocean redox conditions are likely intertwined with the evolution of the overall Earth system, including the biosphere, crust, and mantle (e.g., Holland, 2006; Canfield et al., 2007; Dahl et al., 2010; Lyons et al., 2014; Kendall et al., 2015; Reinhard et al., 2016; Wallace et al., 2017; Lu et al., 2018). Although the modern atmosphere and ocean are well-oxygenated, the environment of the Precambrian was likely different – more widespread anoxic conditions (e.g., Scott et al., 2008; Partin et al., 2013; Lyons et al., 2014; Lu et al., 2017a; Lu et al., 2018; Sheen et al., 2018; Wang et al., 2018). Both environmental (e.g., oxygen level, climate change) and ecological/genetic factors (e.g., arms race) could influence metazoan evolution (e.g., Rhoads and Morse, 1971; Diaz and Rosenberg, 1995; Dahl et al., 2010; Mills and Canfield, 2014; Planavsky et al., 2014; Reinhard et al., 2016). It has been demonstrated a physiological control of O_2 on the body size of species, diversity of carnivory, and complexity of food webs (e.g., Dahl and Hammarlund, 2011; Payne et al., 2011; Sperling et al., 2013; Mills and Canfield, 2014). Therefore, exploring the Earth's surface oxygenation through time greatly helps to understand how metazoans diversified through time and how the Earth evolved as a complex system (e.g., Holland, 2006; Canfield et al., 2007; Butterfield, 2009; Dahl et al., 2010, 2017b, 2019; Reinhard et al., 2013; Lyons et al., 2014; Kendall et al., 2015; Wallace et al., 2017; Lu et al., 2018; Zhang et al., 2019).

Tracking the Earth's oxygenation history is not straightforward and is often inferred from geochemical redox proxies, such as the concentrations and isotopic compositions of redox-sensitive trace metals (e.g., Scott et al., 2008; Partin et al., 2013; Kendall et al., 2015; Lu et al., 2017a; Sheen et al., 2018). The molybdenum and uranium

isotope compositions of euxinic organic-rich mudrocks (ORM) have been widely used as novel global ocean redox tracers (e.g., Barling et al., 2001; Arnold et al., 2004; Stirling et al., 2007; Weyer et al., 2008; Kendall et al., 2009, 2015, 2020; Dahl et al., 2010, 2011; Asael et al., 2013; Lu et al., 2017b; Yang et al., 2017; Wang et al., 2018; Gilleaudeau et al., 2019; Ostrander et al., 2019a). Both Mo and U have much longer modern oceanic residence times (Mo: 440 kyr; U: 400-500 kyr) than the ocean mixing time (~1-2 kyr) (Ku et al., 1977; Dunk et al., 2002; Miller et al., 2011). These metals are soluble and show conservative behavior in oxygenated waters and can be removed to sediments under anoxic conditions via different mechanisms (see Section 2; Anderson, 1989; Barnes and Cochran, 1990; Helz et al., 1996, 2011; Morford and Emerson, 1999; Erickson and Helz, 2000; Dunk et al., 2002; McManus et al., 2006; Algeo and Tribovillard, 2009). The Mo and U isotope compositions of ORMs are sensitive to the extent of global ocean euxinia, and geochemical models have been developed to quantitatively constrain the contemporaneous global ocean redox conditions (e.g., Dahl et al., 2011; Goldberg et al., 2016; Gilleaudeau et al., 2019).

Depending on only Mo isotope compositions of euxinic ORM leads to uncertainty when reconstructing paleocean redox conditions (e.g., Arnold et al., 2004; Neubert et al., 2008; Gordon et al., 2009). Only under strongly euxinic bottom water conditions ($[H_2S]_{aq}$ > 11μM) and near-quantitative removal of Mo from bottom waters can the Mo isotope compositions of modern euxinic sediments approach the global seawater Mo isotope composition (Barling et al., 2001; Arnold et al., 2004; Neubert et al., 2008; Nägler et al., 2011; Noordmann et al., 2015; Bura-Nakić et al., 2018). In contrast, much larger and variable Mo isotope fractionations (0.5-3.0‰) between modern seawater and sediments occur when bottom waters are non-euxinic or weakly euxinic ($[H_2S]_{aq}$ < 11μM) (Arnold et al., 2004; Neubert et al., 2008; Poulson et al.,

2006; Poulson Brucker et al., 2009; Goldberg et al., 2012; Kendall et al., 2017). However, there is no valid method to distinguish between strongly and weakly euxinic conditions for ancient ORM. Therefore, it is challenging to determine how much seawater Mo isotope variation occurred during deposition of a euxinic ORM stratigraphic unit. Because of this difficulty, the heaviest Mo isotope compositions of a euxinic ORM stratigraphic unit are commonly regarded as a conservative lower limit of coeval seawater Mo isotope compositions for the entire unit (Barling et al., 2001; Arnold et al., 2004; Neubert et al., 2008; Gordon et al., 2009; Dahl et al., 2010; Nägler et al., 2011; Kendall et al., 2015; Brüske et al., 2020). However, doing so limits the utility of the Mo isotope system as a global ocean redox tracer.

Inferring ancient global ocean redox conditions solely based on the U isotope compositions of euxinic ORM can also be ambiguous (e.g., Andersen et al., 2014; Rolison et al., 2017; Wang et al., 2018; Brüske et al., 2020; Kendall et al., 2020). A large apparent U isotope fractionation factor between bottom waters and euxinic sediments (≥ 0.6‰) is found to be accompanied by both abiotic and biotic U reduction (U[VI] to U[IV]) and removal, resulting in the preferential accumulation of ^{238}U in U(IV) in sediments as observed in modern euxinic basins (Stirling et al., 2007; Weyer et al., 2008; Montoya-Pino et al., 2010, 2011; Andersen et al., 2014, 2017; Holmden et al., 2015; Noordmann et al., 2015; Rolison et al., 2017; Bura-Nakić et al., 2018; Brüske et al., 2020). This process is explained as the nuclear field shift fractionation (e.g., Bigeleisen, 1996; Schauble, 2007; Abe et al., 2008). However, the effective U isotope fractionation between euxinic bottom waters and sediments can be variable due to changes in the local depositional environment (e.g., aqueous U species, site of U reduction (above, at, or below sediment-water interface [SWI]), the efficiency of U removal, U diffusive-reactive process, sedimentation rate, productivity), limiting the

use of U isotope compositions from ancient ORM to reconstruct global paleocean redox conditions (Andersen et al., 2014, 2017; Noordmann et al., 2015; Rolison et al., 2017; Brown et al., 2018; Bura-Nakić et al., 2018; Brüske et al., 2020; Lau et al., 2020).

Using a single metal isotope system can lead to significant uncertainties; however, the combined use of multiple metal isotope systems is a better approach to more robustly infer ancient seawater metal isotope compositions and thus infer global ocean redox conditions. In this study, we use new and previously published data to further develop the coupled use of Mo and U isotope compositions from Proterozoic and Phanerozoic euxinic ORM to reconstruct global ocean redox conditions. Different patterns of covariation between Mo and U isotope data from individual ORM units are observed, shedding light on the relative influence of local depositional effects versus global redox controls. In addition, the potential ranges of contemporaneous seawater Mo and U isotope compositions during ORM deposition are estimated using a coupled Mo-U isotope model developed from observations of modern marine sediments.

2. THE MOLYBDENUM AND URANIUM ISOTOPE SYSTEMS AS GLOBAL OCEAN REDOX TRACERS

2.1 The Mo isotope proxy

Molybdenum is mainly sourced from the oxidative weathering of the upper continental crust and delivered to the oceans via rivers, and low-temperature seafloor hydrothermal systems contribute a small amount of Mo (~5-10%) to the oceans (McManus et al., 2002; Miller et al., 2011; Reinhard et al., 2013). In the oxygenated surface waters, Mo mainly exists as soluble molybdate (MoO_4^{2-}), which can be slowly adsorbed on the surface of Mn oxides (Barling et al., 2001; Siebert et al., 2003; Barling

and Anbar, 2004). In anoxic and sulfidic environments, the soluble molybdate can efficiently react with aqueous hydrogen sulfide ($[H_2S]_{aq}$) to form particle reactive thiomolybdate and polysulfide species that are scavenged by organic matter and solid sulfide minerals (Helz et al., 1996, 2011; Morford and Emerson, 1999; Erickson and Helz, 2000; Dahl et al., 2013, 2017a). The Mo removal rates in euxinic settings are much higher than in oxic settings (Bertine and Turekian, 1973; Emerson and Huested, 1991; Scott et al., 2008). The redox sensitive behavior and long oceanic residence time (~440 kyr today) make Mo an ideal tracer for global ocean redox conditions (Barling et al., 2001; Miller et al., 2011; Kendall et al., 2017).

The modern ocean has a homogenous δ^{98}Mo of ~2.34 ± 0.10‰ (2SD; Barling et al., 2001; Nakagawa et al., 2012; Nägler et al., 2014). The δ^{98}Mo of low-temperature seafloor hydrothermal systems is estimated around 0.8‰, but is still poorly understood (McManus et al., 2002; Kendall et al., 2017). The weight-averaged δ^{98}Mo of large rivers is estimated to be ~0.7‰ (Archer and Vance, 2008). However, groundwater could potentially contribute a larger amount of Mo to the rivers than previously thought (Moore, 1996). Taking the groundwater input into consideration, the newly estimated average δ^{98}Mo of the riverine inputs is similar to the estimated average composition of the upper continental crust (0.3-0.6‰; Voegelin et al., 2014; King et al., 2016; Willbold and Elliott, 2017; King and Pett-Ridge, 2018). Neely et al. (2018) estimated a δ^{98}Mo value of ~0.5‰ for the overall oceanic Mo inputs, including contributions from rivers, groundwaters, and low-temperature hydrothermal systems.

Under well-oxygenated bottom waters, Fe-Mn oxides are characterized by an average δ^{98}Mo of −0.7‰, indicating a large Mo isotope fractionation of ~3‰ during Mo adsorption to Fe-Mn oxides (Barling et al., 2001; Siebert et al., 2003; Barling and Anbar, 2004). By contrast, continental margin sediments, deposited under weakly

oxygenated and anoxic bottom waters where aqueous hydrogen sulfide is restricted to the porewaters, have a much heavier δ^{98}Mo value of 1.6-2.1‰ (Poulson et al., 2006; Siebert et al., 2006; Poulson Brucker et al., 2009; Eroglu et al., 2020). Sediments deposited in mildly oxygenated environments have intermediate δ^{98}Mo values between −1.0‰ and +1.6‰, which are influenced by the different compositions of Fe and Mn oxides and the levels of $[H_2S]_{aq}$ in the porewaters (Siebert et al., 2006; Goldberg et al., 2009, 2012).

When the bottom water is strongly euxinic ($[H_2S]_{aq}$ > 11 μM, "active point of switch" [APS]), molybdate can be completely converted to trithiomolybdate ($MoOS_3^{2-}$) or tetrathiomolybdate (MoS_4^{2-}) (Helz et al., 1996; Erickson and Helz, 2000). If quantitative Mo removal was further achieved, the authigenic Mo isotope composition of the euxinic sediment is close to that of the open-ocean seawater value as observed in the deep Black Sea and the Kyllaren Fjord (Barling et al., 2001; Neubert et al., 2008; Helz et al., 2011; Noordmann et al., 2015). However, if Mo removal was incomplete (e.g., bottom water renewal rate > Mo burial rate), a small Mo isotopic offset (0.5 ± 0.3‰) between seawater and the euxinic sediments could still occur even in a strongly euxinic environment (Nägler et al., 2011; Bura-Nakić et al., 2018). In contrast, large and variable Mo isotope fractionations (up to ~3‰) could occur under weakly euxinic bottom water conditions ($[H_2S]_{aq}$ < 11 μM) due to the formation of intermediate thiomolybdate species and non-quantitative Mo removal from bottom waters (Arnold et al., 2004; Neubert et al., 2008; Nägler et al., 2011). Short-term redox fluctuations (possibly associated with eustatic sea-level change, occasional inflow of oxygenated waters) could stimulate cycling of the Fe-Mn oxides that shuttle isotopically light Mo to deeper waters or the sediment surface, which can also cause lower δ^{98}Mo in these euxinic sediments as observed in the Cariaco Basin and the Baltic Sea (Gotland Deep

and Landsort Deep) (Huckriede and Meischner, 1996; Dellwig et al., 2010, 2012; Arnold et al., 2004; Goldberg et al., 2009, 2012; Nägler et al., 2011; Scholz, 2013, 2018; Noordmann et al., 2015).

In this framework, during expanded ocean euxinia, the seawater would be characterized by a relatively lower Mo isotope composition due to less removal of isotopically light Mo to oxic sediments. In contrast, a widespread oxygenated ocean would have a higher Mo isotope composition.

2.2 The U isotope proxy

Riverine input is the only known major source of U to the oceans (Dunk et al., 2002). Groundwaters, as an important source of Mo to the oceans, might contribute to oceanic U although it is currently a knowledge gap. Uranium mainly exists as the Ca/Mg-UO_2-CO_3 complexes in oxygenated waters (Langmuir, 1978; Anderson et al., 1989; Dunk et al., 2002; Endrizzi et al., 2016). Unlike Mo removal that can occur in a euxinic water column, U removal typically involves the diffusion of seawater U(VI) into porewaters and subsequent reduction of soluble U(VI) to insoluble U(IV) at the SWI or within the sediments under anoxic conditions (Anderson et al., 1989; Barnes and Cochran, 1990, 1993). The strong negative correlation (r^2 = 0.99) between dissolved U concentrations and hydrogen sulfide concentrations in the Black Sea water column indicates U removal is more efficient when euxinia is more intense (Rolison et al., 2017). It has also been demonstrated that the U reduction and removal rate is proportional to the sulfate reduction rate (Barnes and Cochran, 1993). The U burial rates in euxinic settings are much higher than in oxic settings (Barnes and Cochran, 1990; Morford and Emerson, 1999; Dunk et al., 2002). Oxygenated modern seawater has an average $\delta^{238}U$ of −0.39 ± 0.04‰ (2SD; Stirling et al., 2007; Weyer et al., 2008;

Tissot and Dauphas, 2015; Andersen et al., 2016; Noordmann et al., 2016). The weighted average $\delta^{238}U$ of rivers has been estimated between −0.34‰ and −0.24‰, which is similar to the upper continental crust (−0.3‰; Stirling et al., 2007; Weyer et al., 2008; Tissot and Dauphas, 2015; Andersen et al., 2016; Noordmann et al., 2016).

The U reduction and removal process below the SWI is accompanied by a large and variable U isotope fractionation (typically 0.6-0.8‰) between modern euxinic sediments and bottom waters (Stirling et al., 2007; Weyer et al., 2008; Montoya-Pino et al., 2010; Andersen et al., 2014, 2016; Holmden et al., 2015; Noordmann et al., 2015, 2016; Rolison et al., 2017; Bura-Nakić et al., 2018; Brüske et al., 2020). This diffusive-reactive process for U has been fully explained in previous studies (Clark and Johnson, 2008; Andersen et al., 2014; Rolison et al., 2017; Wang et al., 2018), and thus is only briefly described here. When dissolved U(VI) diffuses across the SWI from bottom waters to sediments, partial U reduction and removal will cause authigenic U accumulation and preferential enrichment of ^{238}U in the sediments, leading to lower U concentrations and lower $\delta^{238}U$ in the porewaters. When U reduction occurs at greater depths below the SWI, there will be progressively less U isotopic offset from overlying seawater because of less dissolved U(VI) in the porewaters (Clark and Johnson, 2008; Andersen et al., 2014; Rolison et al., 2017; Wang et al., 2018).

The full range of intrinsic U isotope fractionation during reduction of U^{6+} to U^{4+} is not well determined. Theoretical calculations based on ab initio molecular orbital modeling suggest an intrinsic U isotope fractionation of 0.95‰ (Abe et al., 2008). Laboratory experimental studies yield a similar value of ~1.0-1.3‰ for abiotic and biotic U reduction (Basu et al., 2014; Stirling et al., 2015; Stylo et al., 2015; Brown et al., 2018). Based on a model that describes Se diffusion and reduction below the SWI, the effective Se isotope fractionation between the dissolved phase and reduced phase is

calculated to be half of the intrinsic Se isotope fractionation (Clark and Johnson, 2008). Similarly, this diffusive-reactive approach can be used for U (Andersen et al., 2014). An effective U isotope fractionation of ~0.6‰ between euxinic bottom waters and sediments is observed in several modern anoxic basins (e.g., the Black Sea, Cariaco Basin, Saanich Inlet, Kyllaren Fjord, Lake Rogoznica; Andersen et al., 2014; Noordmann et al., 2015; Holmden et al., 2015; Rolison et al., 2017; Bura-Nakić et al., 2018; Brüske et al., 2020). This value also matches calculations by a simple Rayleigh model based on studies of modern anoxic basins (Andersen et al., 2014; Rolison et al., 2017; Bura-Nakić et al., 2018; Brüske et al., 2020). Therefore, the intrinsic U isotope fractionation could reach 1.2‰ using an effective U isotope fractionation of 0.6‰ (Clark and Johnson, 2008; Andersen et al., 2014). This intrinsic U isotope fractionation value (1.2‰) is similar to theoretical predictions (Abe et al., 2008) and laboratory studies (Basu et al., 2014; Stirling et al., 2015; Stylo et al., 2015; Brown et al., 2018). In addition, a few anomalously high U isotope compositions were reported for ancient ORMs, such as the Neoarchean Albitibi Formation (up to 0.81‰, leaches; Wang et al. 2018) and Paleoproterozoic Zaonega Formation (up to 0.79‰, whole rock; Mänd et al. 2020), implying large U isotope fractionations (likely > 0.6‰) from coeval seawater. In this study, an intrinsic U isotope fractionation of 1.2‰ is tentatively used.

The depositional environment significantly influences the effective U isotope fractionation factor associated with U reduction and removal to sediments. Taking the U reduction pathway as an example, if U reduction primarily occurred on the sediment surface and was less affected by diffusive-reactive process, the effective U isotope fractionation would be close to the intrinsic U isotope fractionation (Andersen et al., 2017). In addition, generally smaller U isotopic offsets occur in more severely restricted basins due to basin reservoir effect (Andersen et al., 2017; Rolison et al., 2017; Lau et

al., 2020). Besides the U reduction pathway and basin reservoir effect, the magnitude of U isotope fractionation in euxinic settings is influenced by several other factors, such as aqueous U species, aqueous major ion chemistry, basin geometry, bottom water chemistry, sedimentation rate, and productivity (e.g., Andersen et al., 2014, 2018; Noordmann et al., 2015; Rolison et al., 2017; Brown et al., 2018; Bura-Nakić et al., 2018; Tissot et al., 2018; Brüske et al., 2020; Lau et al., 2020).

Ferruginous settings, which were prevalent in the Precambrian (e.g., Planavsky et al., 2011; Poulton and Canfield, 2011; Lowenstein et al., 2014), could be an important sink of U (Cole et al., 2020). A recent study suggests highly variable $\delta^{238}U$ in ancient and modern ferruginous settings, but the average U isotope composition of modern ferruginous sediments is indistinguishable from the adjacent oxic settings (Cole et al., 2020). More studies are needed to further constrain U behavior in ferruginous settings.

In modern oxic and suboxic settings, the U isotope fractionations are much smaller compared with those in euxinic settings (Weyer et al., 2008; Tissot and Dauphas, 2015; Andersen et al., 2016; Cole et al., 2020). The oxygenated Fe-Mn crusts have lighter $\delta^{238}U$ (−0.59‰ to −0.69‰) that is ~0.25‰ on average lower than that of seawater (Goto et al., 2014; Wang et al., 2016). It indicates that ^{235}U is preferentially adsorbed to Fe-Mn crusts, leaving seawater enriched in^{238}U. In the continental margin of Peru and Washington State (United States), sediments deposited under suboxic bottom waters contain $\delta^{238}U$ that are only 0.1-0.2‰ heavier than seawater (Weyer et al., 2008; Tissot and Dauphas, 2015; Andersen et al., 2016). Primary biogenic carbonates contain $\delta^{238}U$ values that approach the modern seawater value, with a small isotope fractionation of < 0.1‰ (Weyer et al., 2008; Romaniello et al., 2013; Chen et al., 2018b). However, modern shallow-water carbonate sediments from the Bahamas bank have higher U concentrations and isotopic compositions (0.24 ± 0.14‰, 1SD)

mainly due to U reduction in the sulfidic sediment pore fluids and aqueous U speciation-dependent isotope fractionations (Romaniello et al., 2013; Chen et al., 2018a, Tissot et al., 2018, Dahl et al., 2019). Negligible U isotope fractionation is observed between seawater and high-temperature hydrothermal alteration of oceanic crust, whereas the $\delta^{238}U$ of crust altered by low-temperature hydrothermal fluids is approximately 0.25‰ higher than that of seawater (Tissot and Dauphas, 2015; Andersen et al., 2015, 2016; Noordmann et al., 2016).

The basic logic of interpreting $\delta^{238}U$ from ORM for the extent of ancient ocean oxygenation/euxinia is based on the modern marine U isotope cycle. During an expansion of ocean euxinia, ^{238}U is preferentially removed to sediments, thus leading to a lighter seawater U isotope composition (enriched in ^{235}U). On the contrary, with increased ocean oxygenation, the preferential removal of ^{238}U from the oceans to euxinic sediments is largely reduced, resulting in a heavier seawater U isotope composition.

2.3 Covariations of $\delta^{98}Mo$ and $\delta^{238}U$ in modern euxinic sediments

Bura-Nakić et al. (2018) compiled sedimentary authigenic average Mo and U isotope compositions of euxinic organic-rich sediments from modern basins and observed an overall negative correlation between the Mo and U isotope data (Figure 1). The apparent ratio of the isotopic fractionation factors of Mo to U ($\Delta^{98}Mo : \Delta^{238}U \approx -0.9‰ : 0.6‰ \approx -3 : 2$) in the euxinic sediments from Kyllaren Fjord, Lake Rogoznica, Cariaco Basin, and Saanich Inlet is approximately −1.5 (Bura-Nakić et al., 2018). This pattern is not suitable for the Black Sea sediments (Unit I), which may be due to sluggish ventilation and renewal of the strongly euxinic deep bottom waters (Bura-Nakić et al., 2018). This causes more efficient Mo removal relative to U such that the

Mo isotope compositions of euxinic sediments in the Black Sea approaches global seawater whereas there are still U isotope fractionations due to kinetically slower U removal (than Mo) and diffusive-reactive processes (Andersen et al., 2014; Rolison et al., 2017; Brüske et al., 2020; Lau et al., 2020).

The inverse correlations between Mo and U isotope compositions are also shown in sediments from several individual euxinic basins (Andersen et al., 2018; Brüske et al., 2020). The $\Delta^{98}Mo$: $\Delta^{238}U$ ratios of the coupled Mo-U isotope data in sediments from the Black Sea (the Unit I, II, and core 32MUC24 sediments), the Cariaco Basin (> 10 cm below the SWI), and the Eastern Mediterranean Sea (Sapropel S5) are −1.19 ± 0.32 (1SE), −1.74 ± 0.33 (1SE), and −2.63 ± 0.57 (1SE), respectively (Barling et al., 2001; Weyer et al., 2008; Montoya-Pino et al., 2010, 2011; Arnold et al., 2012; Andersen et al., 2018; Brüske et al., 2020). The ratios yielded from the Black Sea and Cariaco Basin sediments (Brüske et al., 2020) are close to the ratio inferred from Bura-Nakić et al. (2018), whereas the Sapropel S5 of Eastern Mediterranean Sea has a lower ratio (Andersen et al., 2018). These observations suggest that different depositional conditions for each basin can cause different individual $\Delta^{98}Mo$: $\Delta^{238}U$ ratios. Overall, the local depositional environment (e.g., particulate shuttle, the degree of basin restriction, basin geometry, and dissolved sulfide concentrations) is the major control on the Mo-U isotope data in modern euxinic basins such that the observed negative correlations between the two isotope systems are not related to changes in global ocean redox conditions (Figure 1; Andersen et al., 2018; Bura-Nakić et al., 2018; Brüske et al., 2020).

The Fe-Mn oxide shuttle should also be mentioned because it can significantly influence the $\delta^{98}Mo$ but has little influence on the $\delta^{238}U$ of the sediments (Figure 1; Barling et al., 2001; Weyer et al., 2008; Noordmann et al., 2015; Scholz et al., 2018).

For example, the Landsort Deep sediments deposited < 6 cm below the SWI and Gotland Deep sediments deposited > 20 cm below the SWI of the Baltic Sea were strongly affected by the delivery of Fe-Mn oxides to the seafloor during the inflow of oxygenated waters, and have low δ^{98}Mo of −0.03 ± 0.20‰ (1SD) and −0.15 ± 0.22‰ (1SD), respectively (Noordmann et al., 2015; Scholz et al., 2018). Although the Fe-Mn oxide shuttle also operates in the Cariaco Basin, the influence of the shuttle is weaker because the δ^{98}Mo (> 0.9‰) of the sediments in the basin are generally higher than that of the Baltic Sea sediments (Arnold et al., 2004; Brüske et al., 2020).

3. SAMPLES AND ANALYTICAL METHODS

We report new U isotope data for 28 samples of late Neoproterozoic to middle Paleozoic ORM formations that were previously measured for Mo isotope compositions and sedimentary Fe speciation (Dahl et al., 2010; Kendall et al., 2015). These samples are from the: ca. 640 Ma Black River Dolomite, ca. 520 Ma Yu'anshan Formation, ca. 500-485 Ma Alum Shale, ca. 465 Ma Almelund Shale, ca. 442 Ma Rastrites Shale, ca. 442 Ma Birkhill Shale, ca. 365 Ma Chattanooga Shale, and ca. 365 Ma New Albany Shale (see Appendix A for geological backgrounds). In this study, we also revisit the coupled Mo-U isotope compositions (i.e., measured on the same samples) reported previously for several other ORM formations, including the ca. 372 Ma Kettle Point Formation (Kendall et al., 2020), ca. 442 Ma Tanezzuft Formation (Stockey et al., 2020), ca. 448 Ma Fjäcka Shale (Lu et al., 2017b), ca. 555 Ma Member IV of the Doushantuo Formation (Kendall et al., 2015), ca. 1360 Ma Velkerri Formation (Kendall et al., 2009; Yang et al., 2017), and ca. 2050 Ma Zaonega Formation (Asael et al., 2013). This compilation of new and previously published data is used in our coupled Mo-U

isotope mass-balance model (section 5.2).

Trace element concentrations and uranium isotope separations were carried out in the clean lab of the Metal Isotope Geochemistry Laboratory at the University of Waterloo. The sample dissolutions and purification of U from the digested sample solutions followed the protocols of Weyer et al. (2008) and Kendall et al. (2013), which are briefly described as follows. A small amount (~100mg) of rock powders were ashed at 550°C for at least 24 hours to remove organic matter. Subsequently, samples were digested by concentrated HF-HNO_3-HCl. Samples were then diluted in 2% HNO_3 and elemental concentrations were measured on an Agilent 8800 triple quadrupole inductively coupled plasma mass spectrometer (QQQ-ICP-MS). The SBC-1 (Brush Creek Shale) and SGR-1b (Eocene Green River Shale) were processed along with the samples to verify instrument accuracy. The Al-normalized enrichment factors (EF) of Mo and U were calculated relative to the post-Archean Australian Shale (PAAS) (EF = $[metal/Al]_{sample}$ / $[metal/Al]_{PAAS}$). The PAAS values for Al, U, and Mo are 10 wt.%, 3.1 µg/g, and 1.0 µg/g, respectively (Taylor and McLennan, 1985).

A weighted amount of ^{236}U-^{233}U double spike (IRMM-3636) was added to each digested sample solution to correct for instrumental mass bias and any U isotope fractionation during the column chemistry. Eichrom® UTEVA resin was used to separate U from sample-spike solutions. The U isotope compositions were measured on a Thermo Scientific Neptune multi-collector ICP-MS at the W.M. Keck Foundation Laboratory for Environmental Biogeochemistry, School of Earth and Space Exploration, Arizona State University. The U isotope compositions are reported against the CRM145 standard:

$$\delta^{238}U\ (‰) = \left[\frac{\left({}^{238}U/_{235}U\right)_{sample}}{\left({}^{238}U/_{235}U\right)_{CRM145}} - 1\right] \times 1000 \text{(I)}$$

Three U isotope standards CRM145, CRM129a, and Ricca were measured during the study and have average $\delta^{238}U$ values of 0.00 ± 0.07‰ (2SD, n = 31), −1.69 ± 0.12‰ (2SD, n = 6), and −0.21 ± 0.05‰ (2SD, n = 6), respectively. The measured average $\delta^{238}U$ for the CRM129a and Ricca standards in this study agree with the long-term average $\delta^{238}U$ reported for CRM129a (−1.71 ± 0.09‰, 2SD, n = 237) and Ricca (−0.22 ± 0.07‰, 2SD, n = 243) at Arizona State University (Yang et al., 2017). The 2SD uncertainty of a sample is reported as either the 2SD uncertainty of sample replicate measurements or 0.08‰ (the average long-term 2SD uncertainty of CRM129a and Ricca), whichever is greater. The reference materials SBC-1 and SGR-1b that were processed through chemistry in the same way along with our samples have $\delta^{238}U$ values of −0.20 ± 0.05‰ (2SD, n = 3) and −0.18 ± 0.09‰ (2SD; n = 3), respectively. The measured $\delta^{238}U$ of SBC-1 is identical to the value of −0.24 ± 0.10‰ (2SD, n = 3) reported by Yang et al. (2017) and −0.21 ± 0.04‰ (2SD, n = 3) reported by Rolison et al. (2017), and the measured $\delta^{238}U$ of SGR-1b is indistinguishable from the value of −0.19 ± 0.05‰ (2SD, n = 3) reported by Yang et al. (2017). Three sample duplicates have statistically identical $\delta^{238}U$ values given 2SD uncertainties.

Detrital contamination could affect the bulk Mo and U isotope compositions of the samples. Therefore, authigenic $\delta^{98}Mo$ ($\delta^{98}Mo_{auth}$, relative to NIST 3134 = 0.25‰) and $\delta^{238}U$ ($\delta^{238}U_{auth}$, relative to CRM 145) are calculated relative to PAAS:

$$\delta^{98}Mo_{auth} = \delta^{98}Mo_{sample} - \left(Al/Mo\right)_{sample} \times \frac{\delta^{98}Mo_{PAAS}/\delta^{98}Mo_{sample}}{\left(Al/Mo\right)_{PAAS} - \left(Al/Mo\right)_{sample}}) \text{ (II)}$$

$$\delta^{238}U_{auth} = \delta^{238}U_{sample} - \left(Al/U\right)_{sample} \times \frac{\delta^{238}U_{PAAS}/\delta^{238}U_{sample}}{\left(Al/U\right)_{PAAS} - \left(Al/U\right)_{sample}} \quad \text{(III)}$$

The Al (10 wt.%), Mo (1.0 μg/g), and U (3.1 μg/g) concentrations of PAAS are assumed to be the detrital Al, Mo, and U concentrations, respectively (Taylor and McLennan, 1985). The detrital δ^{98}Mo and δ^{238}U endmembers are assumed to be 0.3‰ and –0.3‰, respectively (Weyer et al., 2008; Voegelin et al., 2014; Tissot and Dauphas, 2015; Andersen et al., 2016, 2017; Noordmann et al., 2016; Kendall et al., 2017; Wang et al., 2018).

4. RESULTS

The trace metal concentrations and isotope compositions for each ORM sample are shown in Table 1. The Neoproterozoic (Cryogenian) Black River Dolomite has an average $\delta^{238}U_{auth}$ of 0.01 ± 0.04‰ (1SD, n = 5). The Cambrian Yu'anshan Formation (520 Ma) and Alum Shale (500 Ma) have similar $\delta^{238}U_{auth}$ values of −0.01 ± 0.07‰ (1SD, n = 5) and −0.01 ± 0.08‰ (1SD, n = 5), respectively. By contrast, the average $\delta^{238}U_{auth}$ of the Ordovician ORM formations is variable: higher $\delta^{238}U_{auth}$ is observed for the 485 Ma Alum Shale (0.15 ± 0.05‰, 1SD, n = 4) and 442 Ma Birkhill Shale & Rastrites Shale (0.05 ± 0.11‰, 1SD, n = 3) whereas lower $\delta^{238}U_{auth}$ is observed for the 465 Ma Almelund Shale (−0.29 ± 0.00‰, 1SD, n = 2). The Devonian New Albany Shale and Chattanooga Shale have an average $\delta^{238}U_{auth}$ of −0.04 ± 0.08‰ (1SD, n = 3).

In order to provide a complete view of the covariation of Mo and U isotope compositions during euxinic ORM deposition, we compiled the coupled Mo-U isotope data from ancient ORM formations in this (number of formations "m" = 8; Table 1) and previous studies (m = 6; Table A1; Figure 2; the Zaonega Formation [Asael et al., 2013], upper Velkerri Formation [Kendall et al., 2009; Yang et al., 2017], Doushantuo Formation Member IV [Kendall et al., 2015], Fjäcka Shale [Lu et al., 2017b], Tanezzuft

Formation [Stockey et al., 2020], and Kettle Point Formation [Kendall et al., 2020]). Archean ORM samples are not included in this compilation because oxidative weathering and thus the riverine Mo flux to the oceans was much smaller in the Archean and increased significantly following the Great Oxidation Event (GOE) (e.g., Farquhar et al., 2000; Pavlov and Kasting, 2002; Scott et al., 2008; Bekker and Holland, 2012; Lyons et al., 2014). Samples with Mo EF < 2 or U EF < 2 could have large uncertainties in their authigenic δ^{98}Mo or δ^{238}U values, thus these isotope data (left blank) are not considered in the following discussion (Table A1).

Correlation coefficients (r, $-1 \leq r \leq +1$) are calculated to show the relationship between the coupled Mo-U isotope data. We interpret r values between ±0.5 and ±1 as datasets as exhibiting negative (−) or positive (+) correlations between authigenic δ^{98}Mo and δ^{238}U data, whereas no specific correlations if $-0.5 < r < 0.5$. It should be noted that the number of samples in each ORM formation are not equal, thus correlation coefficients could be influenced by an ORM formation if it contains a relatively large number of samples and show specific relationships (e.g., the Doushantuo Formation Member IV). In addition, ORM formations with limited number of samples ($n \leq 5$) do not yield robust correlations even if r is between ±0.5 and ±1 (e.g., the Almelund Shale).

There is an overall lack of correlation between the compiled Mo and U isotope data from these euxinic ORM formations ($r = -0.44$, Figure 2). However, for individual ORM units, the coupled Mo-U isotope data show negative (e.g., the Devonian Kettle Point Formation, $r = -0.88$), positive (e.g., the Ordovician Fjäcka Shale, $r = +0.75$), and no correlations (e.g., the Rhuddadian Tanezzuft Formation [$r = -0.22$], the Paleoproterozoic Zaonega Formation [$r = -0.12$]), suggesting different controlling mechanisms at local and global scales that influenced the preservation of sedimentary Mo and U isotope compositions. The correlation coefficient of the Ediacaran

Doushantuo Formation Member IV is −0.54, suggesting an overall negative correlation. However, the Doushantuo samples can be stratigraphically divided into three groups based on different characteristics of the coupled Mo-U isotope data, implying different controls on the Mo and U isotope compositions for each group.

5. DISCUSSION

5.1 Inferring the seawater Mo and U isotope compositions from the coupled Mo-U isotope data of euxinic sediments

Here, we build upon a method from Dahl et al. (2017b) to estimate potential ranges of seawater Mo and U isotope compositions through the combined use of a coupled Mo-U isotope mass balance model and covariations of the coupled Mo-U isotope compositions observed in modern euxinic sediments.

5.1.1 A coupled Mo and U isotope mass balance model

The coupled Mo-U isotope mass balance model can be used to not only quantitatively constrain the relative proportion of each Mo and U oceanic sink but also to estimate the seawater Mo and U isotope compositions under various global ocean redox conditions, respectively. Assuming a steady state mass-balance for Mo (e.g., Goldberg et al., 2016; Ostrander et al., 2019b) and U (e.g., Andersen et al., 2016; Gilleaudeau et al., 2019) for the modern ocean, the Mo and U input fluxes (F_{IN}) and isotope compositions (δ_{IN}) should be equal to that of the Mo and U outputs (F_{OUT}, δ_{OUT}), respectively:

$$F_{IN} = F_{OUT} \qquad \text{(IV)}$$

$$\delta_{IN} \times F_{IN} = \delta_{OUT} \times F_{OUT} \qquad \text{(V)}$$

Assuming a three-sink model for Mo (euxinic [EUX], sulfidic at depth [SAD], and oxic [OX] sinks) and a two-sink model for U (euxinic [EUX] and other [OTHER] sinks), the isotope mass balance [equation (V)] can be expressed as:

$$\delta_{OUT} \times F_{OUT} = \sum(\delta_i \times F_i) \qquad (VI)$$

where "i" represents each specific sink for Mo and U. Defining "f" as the burial fraction of the total Mo or U sinks [equation (VII)], the sum of "f_i" is 1 [equation (VIII)] and equation (VI) can be rewritten as equation (IX):

$$f_i = {}^{F_i}/_{F_{OUT}},\ (0 \le f_i \le 1) \qquad (VII)$$

$$\sum f_i = 1 \qquad (VIII)$$

$$\delta_{OUT} = \sum(\delta_i \times f_i) \qquad (IX)$$

Further, the isotope composition of each sink i is related to that of the contemporaneous seawater, as shown in equation (X):

$$\delta_{OUT} = \sum[(\delta_{SW} + \Delta_i) \times f_i] \qquad (X)$$

where "δ_{SW}" represents the isotope composition of the seawater, and "Δ_i" represents the net isotopic offset between seawater and each sink i. Combining equations V-X, the Mo and U isotope composition of seawater can be calculated as shown in equations (XI) and (XII), respectively:

$$\delta^{98}Mo_{SW} = \delta^{98}Mo_{IN} - \Delta^{98}Mo_{OX} - \left(\Delta^{98}Mo_{EUX} - \Delta^{98}Mo_{OX}\right) \times f_{Mo\_EUX} - (\Delta^{98}Mo_{SAD} - \Delta^{98}Mo_{OX}) \times f_{Mo\_SAD} \qquad (XI)$$

$$\delta^{238}U_{SW} = \delta^{238}U_{IN} - \Delta^{238}U_{OTHER} - \left(\Delta^{238}U_{EUX} - \Delta^{238}U_{OTHER}\right) \times f_{U\_EUX} \qquad (XII)$$

Rivers, groundwaters, and low-temperature seafloor hydrothermal inputs are the sources of Mo to the oceans. The δ^{98}Mo of the overall modern Mo inputs was estimated to be ~0.5‰ (Neely et al., 2018). Here, we use an average δ^{98}Mo of 0.5 ± 0.2‰ for the oceanic Mo inputs, which is similar to the average upper crust (0.3-0.6‰; Voegelin et al., 2014; Willbold and Elliott, 2017). Assigning an average Mo isotopic offset for the

euxinic settings is difficult because sediments deposited under strongly and weakly euxinic environments are characterized by different Mo isotope fractionations (see Section 2.1). Here, we tentatively assume an average Mo isotopic offset of 0.5 ± 0.3‰ for euxinic settings (Table 2). In the oxic settings, a Mo isotope fractionation of 3.0 ± 0.1‰ is observed and is used in this model (Table 2; Siebert et al., 2003; Barling and Anbar, 2004; Wasylenki et al., 2008). The sulfidic at depth sink is used to describe the environment where dissolved sulfide is restricted to the shallow sediment porewaters and either does not occur or rarely occurs in the bottom waters above the SWI (e.g., the Peru continental margin). The SAD sink consists of both the anoxic sink and mildly oxygenated sink, which are characterized by a Mo isotopic offset of ~0.2-0.8‰ and ~0.8-3.0‰, respectively (Poulson et al., 2006; Siebert et al., 2006; Goldberg et al., 2009, 2012; Poulson Brucker et al., 2009; Eroglu et al., 2020). Molybdenum removal to the anoxic sink is more efficient than Mo removal to the mildly oxygenated sink, indicating a dominant role of the anoxic sink for the SAD sink (Poulson Brucker et al., 2009). Therefore, an average Mo isotopic offset of 0.9 ± 0.2‰ is tentatively used for Mo burial in sediments associated with the SAD sink (Poulson et al., 2006; Siebert et al., 2006; Poulson Brucker et al., 2009).

By using the parameters above, euxinic settings should approximately account for less than 8% of total Mo removal to achieve the modern global seawater Mo isotope composition of 2.34‰. Otherwise, the modern seawater Mo isotope composition can only be achieved by increasing Mo removal to the oxic and euxinic sinks while decreasing Mo removal into the SAD sink, which is unrealistic because the intermediate SAD sink should generally expand along with the expansion of the euxinic sink. Here, 45 ± 10%, 50 ± 10%, and 5 ± 3% of total Mo removal in the modern ocean is used for the oxic, SAD, and euxinic sinks, respectively. These values are generally consistent

with estimates from previous studies (Siebert et al., 2003; Scott et al., 2008; Poulson Brucker et al., 2009; Kendall et al., 2009, 2017; Dahl et al., 2011; Reinhard et al., 2013; Chen et al., 2015). Therefore, applying these parameters (Table 2) in equation (XI), the predicted modern seawater Mo isotope composition is 2.33 ± 0.24‰, which is identical to the measured seawater Mo isotope composition of 2.34 ± 0.10‰ (Barling et al., 2001; Nakagawa et al., 2012; Nägler et al., 2014).

The riverine input is the major U source to the oceans and has an average $\delta^{238}U$ value between −0.34‰ and −0.24‰ that is similar to the average upper crust (Dunk et al., 2002; Tissot and Dauphas, 2015; Andersen et al., 2016, 2017; Noordmann et al., 2016; Wang et al., 2018). Therefore, we use an average $\delta^{238}U$ of −0.29 ± 0.03‰ for the U input. Several factors influence U reduction and removal such that variable U isotope fractionations between sediments and bottom waters are observed in modern euxinic settings (see Section 2.2; Andersen et al., 2014, 2017; Holmden et al., 2015; Noordmann et al., 2015; Rolison et al., 2017; Bura-Nakić et al., 2018; Brüske et al., 2020). We tentatively use 0.60 ± 0.20‰ as the U isotopic offset for the euxinic sink because this value is generally consistent with modern euxinic basins (Holmden et al., 2015; Noordmann et al., 2015; Rolison et al., 2017; Bura-Nakić et al., 2018; Brüske et al., 2020). The "other sink" comprises several sinks, including other reducing environments (suboxic settings, anoxic/ferruginous settings, carbonates with dissolved sulfide in sediment pore fluids, biogenic carbonates, oceanic crust altered by high- and low-temperature hydrothermal fluids, and oxic sediments) (Table 3; Tissot and Dauphas, 2015; Andersen et al., 2016, 2017; Noordmann et al., 2016; Wang et al., 2016; Cole et al., 2020). According to the relative fraction of U removal into each sink (Table 3), an overall weighted U isotopic offset of 0.05 ± 0.09‰ is calculated for the other sink [OTHER], which agrees with previous studies (Weyer et al., 2008; Montoya-Pino

et al., 2010; Andersen et al., 2016; Wang et al., 2016; Dahl et al., 2017b; Yang et al., 2017; Zhang et al., 2018; Gilleaudeau et al., 2019; Stockey et al., 2020).

Using the above parameters, the modern seawater $\delta^{238}U$ of −0.39‰ can be achieved when the euxinic and other sinks comprise 9% and 91% of U removal, respectively. These values are consistent with previous estimates of 5-25% for the euxinic sink and 75-95% for the other sink (Barnes and Cochran, 1990; Morford and Emerson, 1999; Dunk et al., 2002; Tissot and Dauphas, 2015; Andersen et al., 2016). Here, we use 9 ± 6% of U removal for the euxinic sinks and 91 ± 6% for the other sinks (Table 2). Applying these values in equation (XII), the modeled modern seawater has a $\delta^{238}U$ of −0.39 ± 0.10‰ (Table 2), which is in good agreement with the measured $\delta^{238}U$ of modern seawater (−0.39 ± 0.04‰; Weyer et al., 2008; Tissot and Dauphas, 2015; Andersen et al., 2016, 2017; Noordmann et al., 2016).

In order to couple the Mo and U isotope mass balance models, we assume that there is a general correlation between the Mo and U euxinic burial fractions (Dahl et al., 2017b), which can be described as:

$$f_{Mo\_EUX} = f_{U\_EUX}^{\gamma} \qquad \text{(XIII)}$$

Two end-member criteria should be fulfilled for the above equation: 1) if $f_{Mo\_EUX} = 0$, then $f_{U\_EUX} = 0$; 2) if $f_{Mo\_EUX} = 1$, then $f_{U\_EUX} = 1$. Here, $\gamma = 1.24 \pm 0.38$ is calculated using 5 ± 3% and 9 ± 6% as the euxinic burial fraction of Mo and U in the modern ocean, respectively (Table 2; see Figure A1 for sensitivity analysis). This is identical to the previously reported value of 1.34 ± 0.38 by Dahl et al. (2017b), who assumed the fractions of anoxic Mo and U removal in the modern ocean are 6-15% and 12-25%, respectively. Combining equations (XI)-(XIII), the covariations of the seawater Mo and U isotope compositions under various redox conditions are shown in Figure 3a. Each black dot in Figure 3a represent specific seawater Mo and U isotope

compositions that correspond to specific fractions of U removal into the euxinic sink (vertical black dashed lines) and Mo removal into the SAD sink (curved colorful lines).

5.1.2 Estimating the modern seawater Mo and U isotope compositions from the coupled Mo-U isotope mass balance model

The estimation of modern seawater Mo and U isotope compositions here is based on the coupled Mo-U isotope data from modern euxinic settings and the coupled Mo-U isotope mass balance model. Although an effective U isotope fractionation of ~0.6‰ has been proposed for euxinic settings (e.g., Andersen et al., 2014; Bura-Nakić et al., 2018; Brüske et al., 2020), several factors could influence the effective U isotope fractionations and the full range of intrinsic U isotope fractionations is still uncertain (see Section 2.2). Here, we tentatively use 1.2‰ as the intrinsic U isotope fractionation during U^{6+} reduction in euxinic settings (see Section 2.2) because this value is generally consistent with theoretical ab initio modeling calculations (Abe et al., 2008) and laboratory experiments (Stirling et al., 2015; Stylo et al., 2015; Brown et al., 2018). Assuming the inverse correlation between Mo and U isotope compositions in modern euxinic settings ($\Delta^{98}Mo : \Delta^{238}U \approx -3 : 2$; Bura-Nakić et al., 2018) is still effective at the full range of intrinsic U isotope fractionation of 1.2‰, the corresponding range of Mo isotope fractionation would be 1.8‰. We acknowledge that this linear relationship is not confirmed by experiments and needs further studies.

This linear relationship is used to account for variable U isotope fractionations between open ocean seawater and euxinic sediments caused by local depositional environments (e.g., dotted and dashed lines in Figure 3b; see Section 2.2). For the curve, symbol "X" represents the best estimate of modern seawater Mo and U isotope compositions. The regression line with a negative slope is defined by Mo-U isotope

data from euxinic basins without severe restriction from the open ocean, whereas the line that intersects the Black Sea sediments represents the case of strong basin restriction (Figure 3b and 3c).

Our approach for estimating the δ^{98}Mo and δ^{238}U of modern seawater is to extrapolate the curve inferred from modern euxinic environments (Bura-Nakić et al., 2018) to the coupled Mo-U isotope mass balance model solutions, in which unrealistic solutions for the modern ocean (e.g., Mo removal in EUX is larger than SAD) are excluded (Figure 3b). Two scenarios are applicable here: samples deposited in non- or weakly-restricted basins vs strongly restricted basins. Using the Mo-U isotope data of sediments deposited with no severe basin restrictions and no significant influence of the Fe-Mn particulate shuttle (e.g., the Cariaco Basin), the symbol "X" of the dotted and dashed curves should be moved along the negative regression line to reach the model solution space. The dotted and dashed curves represent maximum and minimum U isotope fractionations, respectively (Figure 3b). Therefore, the modern seawater Mo and U isotope compositions are estimated to be 2.25‰ to 2.55‰ and −0.51‰ to −0.34‰, respectively (Figure 3b). On the other hand, if there was strong basin restriction during sediment deposition (e.g., Black Sea Unit I), the euxinic sediments potentially have seawater-like Mo isotope compositions and the curve should be moved horizontally to reach the model solution space (solid curves in Figure 3c; Bura-Nakić et al., 2018). In this case, the modern seawater is estimated to have δ^{98}Mo of ~2.37‰ and δ^{238}U from −0.50‰ to −0.34‰. The estimated δ^{98}Mo and δ^{238}U of modern seawater from both cases are similar to the measured δ^{98}Mo (2.34 ± 0.10‰) and δ^{238}U (−0.39 ± 0.04‰) values of modern seawater, respectively (Barling et al., 2001; Weyer et al., 2008; Nakagawa et al., 2012; Nägler et al., 2014; Tissot and Dauphas, 2015; Andersen et al., 2016; Noordmann et al., 2016; Bura-Nakić et al., 2018).

5.1.3 Estimating the ancient seawater Mo and U isotope compositions based on euxinic ORMs from the coupled Mo-U isotope mass balance model

To reconstruct ancient seawater Mo and U isotope compositions, there are a few assumptions for the use of the coupled Mo-U isotope mass balance model. We assume that: 1) steady state conditions were achieved during ancient ORM deposition, particularly for a long period of geologic time and not perturbed by post-depositional processes; 2) the post-Archean Mo and U oceanic inputs have similar δ^{98}Mo (0.5 ± 0.2‰) and δ^{238}U (−0.29 ± 0.03‰) values as today; 3) the magnitudes of net Mo and U isotopic difference between each defined sink and coeval seawater are similar to those observed in modern observations; 4) the relationship between Mo and U isotope compositions of ancient euxinic ORM are similar to that inferred from multiple modern euxinic basins, though inverse Mo-U isotope correlations can have slopes that are different in the individual basins.

Applying the coupled Mo-U isotope mass balance model to ancient euxinic ORMs needs to be discussed in two cases: ORMs (not affected by a Fe-Mn oxide shuttle) deposited in non- or weakly-restricted basins (Figure 4a) vs strongly restricted basin (Figure 4b). Before interpreting the coupled Mo-U isotope data, the local depositional environment should be carefully evaluated. For the conceptual illustrations shown in Figure 4, it is assumed that the ORMs were deposited under euxinic conditions and were not significantly affected by a particulate Fe-Mn oxide shuttle. If the ORMs were deposited when basin restriction was not severe, then the negative regression line (curve 1 and 2) should be placed at sample A (the lowest $\Delta^{238}U/\Delta^{98}Mo$ ratio) and then extrapolated to solution boundaries (yellow area, Figure 4a). Curve 1 and 2 represent the minimum and maximum isotope fractionations from coeval seawater, respectively

(Figure 4a). The U isotopic offset between samples and the best estimate for seawater $\delta^{238}U$ (symbol "X") should be within the range of the intrinsic U isotope fractionation for euxinic settings (1.2‰). Curve 3 is by moving curve 2 up vertically and stopping at where the negative regression line crosses the sample B (the highest $\Delta^{238}U/\Delta^{98}Mo$ ratio) (Figure 4a). This movement ensures that all samples are bracketed between the two negative regression lines and the U isotopic offsets between the samples and seawater are within 1.2‰. The model solution space (highlighted area) encompassed between the two negative regression lines represents the potential range of contemporaneous seawater Mo and U isotope compositions during ORM deposition. Because the highest $\delta^{98}Mo$ from a set of euxinic samples from the same formation represents the most conservative estimate of seawater Mo isotope composition (white dotted horizontal line), in this case, the upper highlighted blue area (above the white dotted line) in Figure 4a represents the potential range of coeval seawater isotope compositions. For the ORMs deposited in strongly restricted basins, assuming there was no variation in seawater $\delta^{98}Mo$ during deposition, only the sample with the highest $\delta^{98}Mo$ is used because this $\delta^{98}Mo$ value likely approached the coeval seawater Mo isotope composition (Figure 4b). Therefore, curve 1' is moved laterally to curve 2' and the best estimate of the seawater U isotope composition is between the "X" symbols of both curves (Figure 4b). However, with a data distribution that is shown in Figure 4b, it is not possible to know if seawater $\delta^{98}Mo$ was constant or variable because a combination of local and global changes could cause a scattered data distribution. For simplicity, only curve 1 and 3 in Figure 4a and curve 2' in Figure 4b (assuming there were no seawater $\delta^{98}Mo$ variations during deposition) are used for weak and strong basin restrictions, respectively, when discussing application of the model to ancient ORM.

5.2 Covariations of Mo and U isotope compositions in the individual ancient euxinic ORM units: Influence of local depositional environment versus global ocean redox conditions

Although there is no overall correlation between δ^{98}Mo and δ^{238}U of the compiled euxinic ORM formations (r = −0.44), the individual euxinic ORM units exhibit various patterns of coupled Mo and U isotope compositions: a negative correlation for the Devonian Kettle Point Formation (r = −0.88; Kendall et al., 2020), a positive correlation for the Ordovician Fjäcka Shale (r = 0.75; Lu et al., 2017b), and no or weak correlations for the other ORM units (e.g., the Rhuddadian Tanezzuft Formation [r = −0.22; Stockey et al., 2020], the Paleoproterozoic Zaonega Formation [r = −0.12; Asael et al., 2013], the Ediacaran Doushantuo Formation Member IV [r = −0.54; Kendall et al., 2015]). To decipher global ocean redox conditions using the sedimentary Mo and U isotope compositions of ORMs, the local depositional environment needs to be analyzed and understood (e.g., Dahl et al., 2010; Scholz et al., 2013, 2018; Andersen et al., 2014, 2017; Noordmann et al., 2015; Kendall et al., 2015, 2017, 2020; Rolison et al., 2017; Bura-Nakic et al., 2018; Ostrander et al., 2019a; Brüske et al., 2020). Here, the geochemical data, including the Mo/TOC ratios, Mo/U EF ratios, and Fe speciation, together with geological background (e.g., paleogeographic maps), are used to interpret the local depositional environment of ORM formations from this (n = 8; Dahl et al., 2010) and previous studies (n = 6; Kendall et al., 2009, 2015, 2020; Asael et al., 2013; Lu et al., 2017b; Yang et al., 2017; Stockey et al., 2020).

The local bottom water redox condition can be inferred from sedimentary Fe speciation (Poulton and Raiswell, 2002; Poulton and Canfield, 2005, 2011; Canfield et al., 2007; Planavsky et al., 2011; Raiswell et al., 2018). Highly reactive Fe (Fe_{HR})

consists of pyrite Fe (Fe_{py}) as well as the carbonate Fe (Fe_{carb}), ferric oxide Fe (Fe_{ox}), and magnetite Fe (Fe_{mag}) that could react with sulfide during deposition and early diagenesis (Poulton and Canfield, 2005, 2011; Raiswell et al., 2018). The ratio of highly reactive Fe over total Fe (Fe_T) can be used to indicate anoxic ($Fe_{HR}/Fe_T > 0.38$) or oxic ($Fe_{HR}/Fe_T < 0.22$) water columns (Poulton and Canfield, 2011; Raiswell et al., 2018). The Fe_{HR}/Fe_T ratios between 0.22 and 0.38 represent an ambiguous zone of bottom water redox environment. In anoxic bottom waters, the ratio of pyrite Fe over total Fe can further distinguish euxinic ($Fe_{py}/Fe_{HR} > 0.7$-0.8) and ferruginous ($Fe_{py}/Fe_{HR} < 0.7$-0.8) conditions (Poulton and Canfield, 2011; Raiswell et al., 2018).

The Mo/TOC ratios of modern euxinic sediments are suggested to mimic aqueous Mo concentrations in the bottom waters and reflect the rate of bottom water renewal by open-ocean seawater (Algeo and Lyons, 2006). In the modern anoxic basins, euxinic sediments from the strongly restricted Black Sea, the moderately restricted Framvaren Fjord, the less restricted Cariaco Basin, and the relatively open Saanich Inlet have average Mo/TOC ratios of 4.5 μg/g/wt.%, 9 μg/g/wt.%, 25 μg/g/wt.%, and 45 μg/g/wt.%, respectively (Algeo and Lyons, 2006). Therefore, the comparison of sedimentary Mo/TOC between ancient ORM and modern basins can be used to indicate the degree of basin restriction. However, other factors complicate the use of sedimentary Mo/TOC as a tracer of basin restriction, such as global ocean redox conditions, sedimentation rates, and thermal maturity (e.g., Algeo and Lyons, 2006; Scott et al., 2008; Ardakani et al., 2016; Dickson et al., 2019). For example, a fast sedimentation rate could dilute Mo concentrations in euxinic sediments and cause lower Mo/TOC ratios, thus leading to an incorrect interpretation of a more restricted depositional environment (Sageman and Lyons, 2003). Less oxygenated ancient oceans could have a smaller Mo reservoir than the well-oxygenated modern ocean such that

the deposited ORMs contain lower Mo/TOC ratios without basin restriction (Scott et al., 2008; Asael et al., 2013). The maturation of ORM could cause the loss of TOC, thus leading to an increase of Mo/TOC ratios (Dickson et al., 2019) and scattered Mo-TOC relationships on a cross plot of Mo vs TOC (Ardakani et al., 2016).

The patterns of Mo and U enrichments in sediments can be used to infer the local depositional environment due to the different removal mechanisms of the two metals (Algeo and Tribovillard, 2009). The efficiency of Mo removal to sediments is influenced by the amount of hydrogen sulfide ($[H_2S]_{aq}$) in the water column and the operation of a particulate Fe-Mn oxyhydroxide shuttle (Helz et al., 1996, 2011; Morford and Emerson, 1999; McManus et al., 2006; Algeo and Tribovillard, 2009). In contrast, the efficiency of U removal to sediments is less dependent on dissolved H_2S availability and is more associated with abiotic/biotic reduction and the diffusive-reactive process below the SWI (Anderson, 1989; Barnes and Cochran, 1990; Dunk et al., 2002; McManus et al., 2006; Algeo and Tribovillard, 2009). Therefore, the covariations of Al-normalized Mo and U EF can be used to infer the importance of the Fe-Mn particulate shuttle, bottom water redox conditions, and hydrographic controls on metal enrichment in ORM (Algeo and Tribovillard, 2009). However, the early and middle Proterozoic ORMs have relatively low U concentrations because of dominantly anoxic deep oceans and widespread U removal into anoxic (both euxinic and ferruginous) sediments (Partin et al., 2013). By contrast, Mo removal is mainly associated with the euxinic waters. Therefore, those euxinic ORM could have overall less enrichments of Mo and U but still high Mo/U ratios, which can be incorrectly interpreted as the effect of the particulate shuttle.

After determining the local depositional environment, the contemporaneous ancient seawater Mo and U isotope compositions during ORM deposition can be

estimated based on the coupled δ^{98}Mo-δ^{238}U data of each ORM unit. Applying the curve to fully cover the coupled δ^{98}Mo-δ^{238}U data points of each ORM, the potential ranges of the coeval seawater Mo and U isotope compositions can be revealed by the coupled Mo-U isotope mass balance model (see Section 5.1.3).

5.2.1 Negative correlation between δ^{98}Mo and δ^{238}U: The Kettle Point Formation

The Devonian Kettle Point Formation was deposited in the Appalachian Foreland Basin of an epeiric sea during the Acadian Orogeny (Hamblin, 2010). It is preserved in the "Chatham Sag", which is a structural depression between the Appalachian Basin and Michigan Basin (Hamblin, 2010). The Kettle Point Formation is informally subdivided into units 1 to 4 from the stratigraphic bottom to the top of the formation. Interbedded organic-rich and poor mudstones are found in units 1 and 3 and more uniform intervals of organic-rich mudstones are found in units 2 and 4 (Bingham-Kozlowski et al., 2016). The samples have an average Mo/TOC ratio of 16.1 ± 8.1 μg/g/wt.% (1SD) that is between the Framvaren Fjord (~9 μg/g/wt.%) and the Cariaco Basin (~25 μg/g/wt.%) (Figure 5a; Algeo and Lyons, 2006). High Mo/U EF ratios, together with high Mo and U enrichments (Mo EF: 51.5-644.1, U EF: 3.4-26.7; Figure 5b), suggest a relatively good connection between open-ocean seawater and the local waterbody during the deposition of the Kettle Point Formation (Table A1; Kendall et al., 2020). Although there are no Fe speciation data available, a euxinic depositional environment is indicated by the consistently high Mo/U EF ratios that are three times the modern seawater Mo/U ratio (Algeo and Tribovillard, 2009). In addition, upper unit 4 samples with vanadium EF > 5 may reflect the operation of the Fe-Mn oxide shuttle that is associated with the brackish conditions during deposition (Table A1; Kendall et al., 2020).

The coupled Mo-U isotope data of the Kettle Point Formation ORM show a negative correlation ($r = -0.88$) with a slope of -1.36 ± 0.12 (1SE), which is similar to the proposed negative regression line (a slope of −1.5) based on modern environments (Figure 5c; Bura-Nakić et al., 2018). This observation indicates that changes in local depositional factors (e.g., bottom water sulfide concentrations) influenced the Mo and U isotope compositions of these ORM at a time of relatively stable global seawater redox conditions (Kendall et al., 2020). Upper unit 4 samples that are potentially affected by the Fe-Mn particulate shuttle show a general horizontal trend (relatively invariable δ^{98}Mo and variable δ^{238}U) with a slope of -0.23 ± 0.31 (1SE). However, the influence of a particulate shuttle on the observed low δ^{98}Mo (0.79 ± 0.11‰) of upper unit 4 may not be that significant because the Landsort Deep (-0.03 ± 0.20‰, 1SD; sediments deposited < 6 cm below the SWI) and Gotland Deep sediments (-0.15 ± 0.22‰, 1SD; sediments deposited > 20 cm below the SWI) that are significantly affected by the particulate shuttle have lower Mo isotope compositions (Noordmann et al., 2015; Scholz et al., 2018). In addition, there is no vertical jump of δ^{98}Mo between the upper unit 4 and units 1-3 & lower unit 4, implying that the particulate shuttle does not significantly alter the sedimentary δ^{98}Mo record. Therefore, it is possible that relatively lower and constant bottom water sulfide concentrations associated with increased mixing with fresh waters (brackish conditions) led to a relatively constant Mo isotopic offset between sediment and seawater during upper unit 4 deposition. At the same time, the variable δ^{238}U values of the same samples indicate that the U isotope fractionations are influenced by several other factors such as the aqueous U species and the rates of U reduction and removal (Andersen et al., 2014, 2017; Rolison et al., 2017; Kendall et al., 2020). By contrast, units 1-3 and lower unit 4 samples show a negative correlation between the Mo and U isotope compositions with a slope of -1.78 ± 0.33

(1SE) that is similar to the modern Cariaco Basin (−1.74 ± 0.33, 1SE; Brüske et al., 2020). Dissolved sulfide levels in the bottom waters likely control the efficiency of Mo and U removal into sediments, thus resulting in the observed negative correlation between the Mo and U isotope compositions (Kendall et al., 2020).

The Kettle Point Formation samples are used to estimate the ancient seawater Mo and U isotope compositions during ORM deposition by extrapolating the inverse correlation to the coupled Mo-U isotope mass balance model solution space. Applying our proposed method to all samples, the best estimate of coeval seawater Mo and U isotope compositions during ORM deposition is 2.04‰ to 2.75‰ and −0.61‰ to −0.34‰, respectively (Figure 5c). Similar seawater isotope compositions (δ^{98}Mo: 2.04‰ to 2.75‰, δ^{238}U: −0.70‰ to −0.34‰) are obtained if only units 1-3 and lower unit 4 samples are used. Our predictions are consistent with the estimations (δ^{98}Mo ≥ 2.0‰, δ^{238}U ≤ −0.3‰) from Kendall et al. (2020), which are suggestive of a generally oxygenated global ocean during deposition of the largely Famennian Kettle Point Formation. This interpretation is also consistent with the proposed increase in atmosphere-ocean oxygenation during the Devonian (Dahl et al., 2010; Wallace et al., 2017; Lu et al., 2018).

5.2.2 Positive correlation between δ^{98}Mo and δ^{238}U: The Fjäcka Shale

The Fjäcka Shale is preserved in the Siljan Ring area of central Sweden and was deposited on the margin of the Baltica continent, which was at the equator during the (Katian) Late Ordovician (Cocks and Torsvik, 2005). The Mo/TOC ratios of the Fjäcka Shale (13.2 ± 10.8 μg/g/wt.%, 1SD) are generally between that of the Black Sea (~4.5 μg/g/wt.%) and Cariaco Basin (~25 μg/g/wt.%) (Figure 6a; Table A1; Lu et al., 2017b). A relatively smaller oceanic Mo reservoir in a less oxygenated Katian world compared

to today likely resulted in overall lower Mo/TOC ratios of Katian ORM compared to modern euxinic sediments (Lu et al., 2017b). Therefore, the depositional environment of the Fjäcka Shale is probably no more than moderately restricted, which is in line with high Mo and U enrichments (Mo EF: 14.1-226.9, U EF: 6.2-10.4; Lu et al., 2017b). Euxinic bottom water redox conditions during Fjäcka Shale deposition are inferred from the Fe speciation data, which agrees with the high Mo/U EF ratios (Figure 6b; Table A1; Lu et al., 2017b).

The Fjäcka Shale is an example of an ORM unit with a positive correlation between Mo and U isotope compositions ($r = +0.75$; Figure 6c). In contrast to a negative correlation that is controlled by changes in the local depositional environment, a positive correlation between Mo and U isotope compositions is best explained by a changing global ocean redox state, which shifts seawater Mo and U isotope compositions and thus the sedimentary Mo and U isotope compositions of euxinic ORM in the same direction (see Section 2). Other explanations seem unlikely. The stratigraphically lower and higher Fjäcka Shale samples are characterized by lower δ^{98}Mo (0.42‰ to 0.81‰) and δ^{238}U (−0.23‰ to −0.02‰), whereas samples with higher δ^{98}Mo (0.87‰ to 1.28‰) and δ^{238}U (0.03‰ to 0.14‰) are stratigraphically in the middle (Table A1). Samples with higher δ^{98}Mo and δ^{238}U are from the Stumsnäs #1 core (more continuous sampling over ~4 m) but not the Solberga #1 core (more discrete sampling over ~2 m) possibly because samples from the Solberga #1 core with the same features were missed during sampling (Lu et al., 2017b).

Applying our method, the coeval seawater could have δ^{98}Mo of 1.31‰ to 1.75‰ and δ^{238}U of −0.80‰ to −0.54‰ during the deposition of stratigraphically higher and lower Fjäcka Shale, whereas the global seawater δ^{98}Mo and δ^{238}U could be 1.48‰ to 2.37‰ and −0.69‰ to −0.34‰, respectively, during deposition of the stratigraphically

middle Fjäcka Shale (Figure 6c). Therefore, a transient ocean oxygenation event likely occurred during the deposition of Fjäcka Shale. These seawater estimations assume that the inverse correlation of Mo-U isotope compositions for Ordovician euxinic basins is identical to the overall slope defined by modern euxinic basins. Because individual modern euxinic basins have yielded different slopes between the Mo and U isotope compositions (see Section 2.3), there is some uncertainty associated with estimates of global seawater Mo and U isotope compositions based on ORM data that show a positive Mo-U isotope correlation. By comparison, Lu et al. (2017b) estimated Late Ordovician (Katian) seawater δ^{98}Mo of 1.4‰ to 2.1‰ and δ^{238}U of −0.85‰ to −0.60‰ during Fjäcka Shale deposition. Their estimations were made individually with assumed isotopic offsets. However, they did not recognize the changing global ocean redox conditions through the positively correlated Mo and U isotope compositions. An episode of increased global ocean oxygenation during the Katian Fjäcka Shale deposition is suggested in this study based on the coupled Mo-U isotopes, implying dynamic ocean redox conditions during the Ordovician (and more generally throughout the Early Paleozoic; Dahl et al., 2017b, 2019; Bartlett et al., 2018; Wei et al., 2018).

5.2.3 No correlation between δ^{98}Mo and δ^{238}U

Unlike the two previous examples of negative and positive correlations of Mo-U isotope data for euxinic ORM that are mainly controlled by changes in the local depositional environment and global ocean redox conditions, respectively, the absence of a correlation between δ^{98}Mo and δ^{238}U suggests distinctive local depositional conditions, a more complex combination of local and global controlling mechanisms or is an artifact of limited data. The Tanezzuft Formation, Zaonega Formation, and Doushantuo Formation Member IV have sufficient data and thus will be discussed in

detail, whereas the other ORM units with limited data will only be briefly described.

5.2.3.1 The Tanezufft Formation: relatively stable local and global ocean redox conditions

The (Rhuddanian) early Silurian Tanezzuft Formation was deposited in the intracratonic Murzuq Basin (Libya) during a marine transgression caused by the melting of the Late Ordovician ice sheets (Desio, 1936; Davidson et al., 2000; Lüning et al., 2000). The Mo/TOC ratios of the Tanezzuft Formation (7.2 ± 2.6 μg/g/wt.%, 1SD) are mostly between that of the Black Sea (~4.5 μg/g/wt.%) and Framvaren Fjord (~9 μg/g/wt.%) (Figure 7a; Table A1; Stockey et al., 2020). This low Mo/TOC ratio does not necessarily represent a limited connection between the local watermass and the open ocean because a smaller oceanic Mo reservoir is expected during the ocean anoxic events (e.g., Algeo, 2004; Montoya-Pino et al., 2010), in this case, the Hirnantian-Rhuddanian ocean anoxic event (Hammarlund et al., 2012; Melchin et al., 2013; Bartlett et al., 2018; Zou et al., 2018). The average Mo EF and U EF are 54.3 (8.3-127.7) and 8.2 (2.5-23.3), respectively. The high Mo/U EF ratios that are nearly three times the modern seawater Mo/U ratio suggest a relatively good connection between the local watermass and the open ocean (Figure 7b). Euxinic bottom water conditions are inferred from sedimentary Fe speciation, which is in an agreement with high Mo/U EF ratios (Stockey et al., 2020).

Covariations of the Mo and U isotope compositions of the Tanezzuft Formation are examined (Figure 7c). Narrow ranges are observed for both $\delta^{98}Mo_{auth}$ (0.51 to 0.97‰) and $\delta^{238}U_{auth}$ (−0.18‰ to 0.07‰), suggesting relatively constant Mo and U isotopic offsets between the euxinic ORM and seawater (Stockey et al., 2020). This observation further implies a relatively stable local depositional environment (e.g.,

bottom water redox conditions, basin restriction). The coupled $\delta^{98}Mo_{auth}$ and $\delta^{238}U_{auth}$ data of the Tanezzuft Formation do not exhibit a negative or positive correlation ($r = -0.22$), indicating no significant changes in global ocean redox conditions at the time.

The contemporaneous seawater Mo and U isotope compositions during deposition of the Tanezzuft Formation are estimated by the proposed model and compared with previous studies (Bartlett et al., 2018; Stockey et al., 2020). Applying our method, Rhuddanian seawater is characterized by $\delta^{98}Mo$ of 1.32‰ to 1.95‰ and $\delta^{238}U$ of −0.78‰ to −0.34‰ during deposition of the Tanezzuft Formation (Figure 7c). By comparison, Stockey et al. (2020) did not clearly predict a coeval seawater $\delta^{238}U$ value but estimated Rhuddadian seawater $\delta^{98}Mo$ to be ~0.69 ± 0.13 (1SD) assuming no Mo isotope fractionations between local euxinic ORMs and the open ocean. The broadly co-deposited carbonates (the Becscie Formation) on Anticosti Island (Canada) have an average $\delta^{238}U$ of ~ −0.45‰ (Bartlett et al., 2018). Applying a modern $\delta^{238}U$ offset of 0.24‰ between shallow-water carbonates and seawater to the carbonates of the Becscie Formation, the Rhuddadian seawater likely had a $\delta^{238}U$ value of ~ −0.69‰. Therefore, the $\delta^{238}U$ offset of ~0.67‰ between euxinic Tanezzuft Formation (−0.02 ± 0.07‰, 1SD; Stockey et al., 2020) and the Rhuddadian seawater (~ −0.69‰) inferred from carbonates is generally consistent with observed U isotope fractionations between modern euxinic sediments and open-ocean seawater (e.g., Andersen et al., 2014, 2017; Noordmann et al., 2015; Rolison et al., 2017; Bura-Nakić et al., 2018; Brüske et al., 2020). In summary, our estimated $\delta^{98}Mo$ of Rhuddanian seawater (1.32-1.95‰) is higher than that (~0.69‰) from Stockey et al. (2020) mainly because they assumed no Mo isotopic offset between euxinic ORMs and seawater, whereas our model predicts there was a Mo isotopic offset. Our estimated Rhuddadian seawater $\delta^{238}U$ value has a large range (−0.78‰ to −0.34‰) and is consistent with the estimation (−0.69‰) based

on carbonates of the Becscie Formation (Bartlett et al., 2018).

5.2.3.2 The Zaonega Formation: potentially variable extent of basin restriction

The Zaonega Formation (~2.05 Ga) was deposited in the Onega Basin in a rifted continental marginal area and was deformed and metamorphosed (to low greenschist facies) during the 1.98-1.79 Ga Svecofennian Orogeny (Hannah et al., 2008; Melezhik et al., 1999, 2015). It is still not well understood if the basin was relatively well connected to the open ocean (e.g., Asael et al., 2013; Scott et al., 2014; Mänd et al., 2020) or not (e.g., Qu et al., 2012; Paiste et al., 2018) during deposition of the Zaonega Formation. The Zaonega Formation has low Mo/TOC ratios that are mostly below the modern Black Sea average (4.5 μg/g/wt.%), suggesting a severely restricted environment (Figure 8a; Table A1). However, the low Mo/TOC ratios are also expected for ORM deposited in the less oxygenated Paleoproterozoic oceans where a smaller seawater Mo reservoir than the modern ocean was likely (Scott et al., 2008; Asael et al., 2013; Reinhard et al., 2013). The average Mo and U enrichment factors are 33.9 (6.0-114.8) and 3.1 (1.5-7.2), respectively (Figure 8b). The high Mo/U EF ratios are mostly three times the modern seawater Mo/U ratio, suggesting euxinic bottom waters with the potential effect of an Fe-Mn particulate shuttle on Mo enrichment (Figure 8b). It was previously suggested that the stratigraphically lower part of the section (Unit A and B) was affected by metamorphism, which caused alteration of pyrite to pyrrhotite, whereas the stratigraphically higher part of the section (Unit C) is less metamorphosed (Asael et al., 2013). Euxinic bottom water redox conditions were inferred for samples from Unit C (Asael et al., 2013). Detailed analysis of each specific Fe pool and the similar Mo isotope compositions of all samples raises the possibility that the more metamorphosed samples were also deposited under euxinic bottom waters (Asael et al.,

2013). It has been shown that ancient ORMs that have undergone low greenschist facies metamorphism can still provide robust depositional information, such as precise and accurate Re-Os depositional ages (Kendall et al., 2004; Rooney et al., 2011). Considering the similar redox sensitive behavior between Mo & U and Re & Os, it is likely that the Mo and U isotope compositions of such ORMs (especially less metamorphosed samples in Unit C) reflect the depositional environment.

The coupled Mo-U isotope data from the euxinic samples in less metamorphosed Unit C are used to ensure a more reasonable interpretation of global seawater redox conditions (Figure 8c). The euxinic samples define a horizontal trend of δ^{98}Mo (0.72 ± 0.09‰, 1SD) with a slope of −0.10 ± 0.38 (1SE). This trend is similar to upper unit 4 (δ^{98}Mo = 0.79 ± 0.11‰, 1SD) of the Kettle Point Formation (−0.23 ± 0.31, 1SE), suggesting that Mo isotope compositions were mainly controlled by relatively lower and constant bottom water sulfide concentrations with a potentially minor effect from the Fe-Mn particulate shuttle, whereas the variable U isotope fractionations were influenced by several processes. However, there is one euxinic sample that shows a higher δ^{98}Mo of 1.40 ± 0.11‰ (2SD) compared with other euxinic samples, though the U EF is less than 2 (Figure 8c). The high δ^{98}Mo value could be caused by more quantitative Mo removal when the bottom water renewal rate was slower (Mo/TOC = 1.8 μg/g/wt.%; Asael et al., 2013), which is indicative of a transient period of stronger basin restriction. Therefore, the degree of basin restriction was likely variable during the deposition of Zaonega Formation.

The coeval seawater Mo and U isotope compositions during deposition of the Zaonega Formation is estimated and compared with previous studies (Asael et al., 2013, 2018). Two possible scenarios are examined because of potential changes in the extent of basin restriction: 1) stronger basin restriction for the euxinic sample that has a δ^{98}Mo

of 1.40‰; and 2) relatively open marine environment for the rest of the euxinic samples that have an average δ^{98}Mo of 0.72 ± 0.09‰ (1SD). Applying our method, the first scenario suggests a global seawater δ^{98}Mo of 1.40‰ (horizontal extrapolation to the model curves assuming the local bottom waters were strongly euxinic) and δ^{238}U of −0.66‰ to −0.34‰ (solid line in Figure 8c). By comparison, the second scenario suggests a global seawater δ^{98}Mo of 1.57‰ to 2.37‰ and δ^{238}U of −0.68‰ to −0.34‰ by extrapolating to the model solution space using a curve whose slope is similar to the average slope defined by data from modern euxinic basins (dotted lines in Figure 8c). The current dataset does not allow us to further justify which case best reflects the coeval global ocean redox conditions and it remains possible that both cases may have occurred. In comparison, Asael et al. (2013) estimated that the ca. 2.05 Ga global seawater δ^{98}Mo and δ^{238}U were 0.75 ± 0.21‰ and −0.18 ± 0.15‰, respectively. Recently, more δ^{98}Mo data were obtained for the Zaonega Formation from two additional drillcores and suggested a coeval seawater δ^{98}Mo of 0.70 ± 0.21‰ (Asael et al., 2018), which is identical to the values from Asael et al. (2013). Our estimated seawater δ^{98}Mo in both scenarios are higher than that of Asael et al. (2013) and Asael et al. (2018). The estimated δ^{238}U of contemporaneous seawater in this study has significant uncertainty (a relatively large range of ~0.32‰) and is generally lower than that of Asael et al. (2013).

5.2.3.3 The Doushantuo Formation Member IV: influence of the particulate Fe-Mn oxide shuttle and the potential change of global ocean redox conditions

The Ediacaran Doushantuo Formation was deposited on a passive continental margin (shelf lagoon and shelf margin-slope transition area) of the Yangtze Block (Wang and Li, 2003; Jiang et al., 2003, 2011). The ORM samples of Doushantuo

Formation Member IV have an average Mo/TOC ratio of 28.3 ± 14.2 μg/g/wt.% (except one outlier with a Mo/TOC value of 290.0 μg/g/wt.%) that is higher than the modern Cariaco Basin (25 μg/g/wt.%) (Figure 9a, Table A1, Kendall et al., 2015). The samples are also enriched in Mo (EF: 65.1-592.1, outlier: 960.8) and U (EF: 6.0-59.0), suggesting a relatively good connection between the local watermass and the open ocean during ORM deposition (Figure 9b; Table A1; Kendall et al., 2015). The Mo/U EF ratios of these samples are mostly greater than three times the modern seawater Mo/U ratio, indicating a euxinic depositional environment that led to efficient Mo removal to the sediments relative to U (Figure 9b; Kendall et al., 2015). This interpretation is confirmed by Fe speciation data (Kendall et al., 2015). It is possible that some samples with high Mo/U EF ratios were influenced by the Fe-Mn particulate shuttle (Figure 9b; Algeo and Tribovillard, 2009).

In this study, rather than use the overall trend (r = –0.54), we subdivided the ORM samples into three stratigraphic groups (1-3) from the bottom to top of Member IV based on their different Mo and U isotope compositions. Group 1 contains lower δ^{98}Mo (< 0.40‰) and variable δ^{238}U (0.15-0.61‰) (r = −0.75, n = 27), group 2 has higher δ^{98}Mo (1.12-2.01‰) and a relatively smaller range of δ^{238}U (0.08-0.31‰) (r = +0.41, n = 8), and group 3 is characterized by moderate δ^{98}Mo (0.20-1.01‰) and variable but generally lower δ^{238}U (−0.40‰ to 0.21‰) (r = −1.00, n = 4; Figure 9c and 9d). These stratigraphic divisions suggest multiple controlling mechanisms on the isotopic compositions of euxinic ORM during deposition of Member IV.

Group 1 and 2 samples overlap in δ^{238}U but have different δ^{98}Mo. The overlapping δ^{238}U ranges between these two groups likely reflect different local depositional effects (that influence the efficiency of U removal to sediments) but generally similar global ocean redox states. The more variable δ^{238}U in group 1 could

be caused by different U reduction and removal rates under weakly euxinic bottom waters, whereas the more uniform $\delta^{238}U$ in group 2 is indicative of relatively more efficient U reduction and removal under more strongly euxinic bottom waters. In addition, the $\delta^{238}U$ of group 2 (0.21 ± 0.09‰, 1SD) are similar to those of sediments from the modern Cariaco Basin and Saanich Inlet, indicating a near modern-level of ocean oxygenation if a U isotope fractionation of 0.6‰ was expressed locally between seawater and the euxinic sediments (Andersen et al., 2014; Holmden et al., 2015; Kendall et al., 2015; Brüske et al., 2020). The interpretation of widespread ocean oxygenation is also consistent with high $\delta^{98}Mo$ of the same samples (up to 2.01‰; Kendall et al., 2015). These high $\delta^{98}Mo$ values can be explained by efficient Mo removal under intensified euxinic bottom waters (Kendall et al., 2015).

By contrast, the much lower $\delta^{98}Mo$ of group 1 (−0.19 ± 0.38‰, 1SD) are similar and comparable to that of the sediments from the Landsort Deep (−0.03 ± 0.20‰, 1SD; sediments deposited < 6 cm below SWI) and Gotland Deep (−0.15 ± 0.22‰, 1SD; sediments deposited > 20 cm below SWI) in the Baltic Sea, which reflects Fe-Mn oxide delivery to the sediments during local transient oxygenation events (Noordmann et al., 2015; Scholz et al., 2018). Therefore, it is likely that the Fe-Mn particulate shuttle contributes to the observed low $\delta^{98}Mo$ in group 1 as this process can explain different $\delta^{98}Mo$ but generally similar $\delta^{238}U$ for groups 1 and 2 (Figure 9c). There is a negative correlation between Mo and U isotope compositions in group 1 that suggests changes in the dissolved sulfide concentrations of bottom waters simultaneously affected the Mo and U isotopic offsets between sediments and seawaters (Brüske et al., 2020). The slope (−2.56 ± 0.45, 1SE) of this negative correlation is similar to that of Sapropel S5 from the Eastern Mediterranean Sea (−2.63 ± 0.57, 1SE), which was related to changing bottom water renewal rates with different extents of basin restriction (Andersen et al.,

2018). Hence, both an Fe-Mn particulate shuttle and bottom water sulfide concentrations (possibly associated with variable basin restriction) may play important roles on the covariation of Mo and U isotope compositions in group 1.

Similar and lower δ^{98}Mo values were recently reported for other Doushantuo Formation Members (II, III, IV) (Ostrander et al., 2019a). Bottom water redox conditions, the operation of an Fe-Mn (oxy)hydroxide shuttle, and sea-level changes (that influence the extent of basin restriction) are proposed to influence Mo isotope fractionations between sediments and overlying seawater (Ostrander et al., 2019a).

To sum up, the global ocean redox state was more oxygenated and remained generally the same during the deposition of group 1 and 2, even though the δ^{98}Mo of the two groups are significantly different. Because group 1 samples were significantly influenced by the Fe-Mn particulate shuttle, the group 2 samples are used to estimate the coeval seawater isotope compositions for both group 1 and 2 (Figure 9c). The coeval global seawater δ^{98}Mo and δ^{238}U are estimated from 2.01‰ to 3.10‰ and from −0.64‰ to −0.34‰, respectively (Figure 9c).

The stratigraphically highest group 3 contains only three samples, which have intermediate δ^{98}Mo (0.20-1.01‰) and generally lower δ^{238}U (−0.40‰ to 0.21‰). The Mo and U isotope compositions of these samples exhibit a clear negative correlation (−1.33 ± 0.09, 1SE) that is close to the proposed average negative correlation observed for modern euxinic basins, reflecting a dominant local depositional control on group 3 Mo-U isotope systematics (Figure 9d; Bura-Nakić et al., 2018; Brüske et al., 2020). Applying our method, the contemporaneous seawater during group 3 deposition could have δ^{98}Mo and δ^{238}U of 1.32‰ to 1.60‰ and −0.78‰ to −0.61‰, respectively (Figure 9d). These values suggest an expansion of ocean anoxia (group 3) following an episode of widespread ocean oxygenation (group 1 and 2). Although there are only three

samples in this group, this interpretation is in an agreement with the low $\delta^{238}U$ (−1.2‰ to −0.8‰) reported for carbonates from the overlying Dengying Formation (South China; Zhang et al., 2018) and co-deposited Nama Group (Namibia; Tostevin et al., 2019). The exceptionally low $\delta^{238}U$ values of the carbonates point to widespread global ocean anoxia during the terminal Ediacaran (Zhang et al., 2018; Tostevin et al., 2019).

5.2.3.4 The rest of the ORM formations

The rest of the euxinic ORM formations have small Mo-U isotope datasets, which significantly limits efforts to distinguish the influences of changes in local depositional conditions from global ocean redox variations because only a small part of the whole coupled Mo-U isotopes covariation pattern would be observed. The Almelund Shale was potentially deposited in a restricted environment based on the low Mo/TOC ratios (≤ 2.6 μg/g/wt.%]), low Mo EF (≤ 6.3) and U EF (≤ 2.7), and Fe speciation evidence for locally euxinic bottom waters, but data come from only two samples (Table 1). Except this formation, we tentatively suggest the rest of the ORM units with small datasets were deposited under euxinic bottom waters with no severe basin restrictions and were not significantly affected by an Fe-Mn particulate shuttle, based on geological background and geochemical data (Figure 10; Appendix A.; Kendall et al., 2009, 2015; Dahl et al., 2010; Yang et al., 2017). The estimated ranges of global seawater Mo and U isotope compositions at the time of ORM deposition were plotted in Figure 10 and summarized in Table 4. If the local depositional environment of each ORM were interpreted correctly, the estimated $\delta^{98}Mo$ of coeval seawater are generally higher than that of the contemporaneous euxinic ORM units, implying appreciable Mo isotope fractionation from coeval seawater. However, it is difficult to determine the exact Mo isotopic offset between sediments and seawater because both a

weakly euxinic environment and the particulate shuttle are possible influencing factors that can not be fully distinguished and quantitatively constrained using small datasets. In addition, the estimated ranges of seawater $\delta^{238}U$ are relatively large for most of these small datasets, which makes it difficult to predict the ancient seawater $\delta^{238}U$ due to several influencing factors on effective U isotope fractionations (e.g., bottom water chemistry, aqueous U species, productivity, U diffusion-reactive process; Andersen et al., 2017; Lau et al., 2020).

Even though a larger dataset would be more helpful, there are a few exceptions where limited Mo-U isotope data could still be useful to reveal global ocean redox conditions. For example, the Late Devonian Chattanooga Shale and New Albany Shale contain high Mo (EF: 308.5-489.5) and U (EF: 28.7-50.1) enrichments, high $\delta^{98}Mo$ (e.g., ~2.0‰), and $\delta^{238}U$ (e.g., ~0.2‰). This combination of geochemical signatures represents compelling evidence of widespread ocean oxygenation at the time of ORM deposition. The ~1.36 Ga Velkerri Formation is worth mentioning as well. The contemporaneous seawater Mo isotope composition is estimated to be at least 1.5‰ in this study, which is higher than previous estimates of ~1.0‰ (Arnold et al., 2004; Kendall et al., 2009). If it is correct, then the global ocean at the time may be relatively more oxygenated than previously thought (e.g., Arnold et al., 2004; Kendall et al., 2009; Planavsky et al., 2011). This hypothesis is generally consistent with the interpretation of high Mo (105-112 μg/g; Kendall et al., 2009) and Re (39.0-52.7 ppb; Sheen et al., 2018) concentrations in bulk samples and pyrite trace element abundances (Mukherjee and Large, 2016), which are suggestive of an episode of ocean oxygenation at 1.36 Ga. In addition, recent studies of $\delta^{98}Mo$ and $\delta^{34}S_{py}$ from the ~1.40 Ga Xiamaling Formation (Zhang et al., 2016; Diamond et al., 2018; Wang et al., 2020) and I/Ca from the ~1.44 Ga Tieling Formation (Hardisty et al., 2017) suggest an episode of transient ocean

oxygenation around ~1.4 Ga.

6. CONCLUSIONS

The coupled use of Mo and U isotope compositions from euxinic ORMs is further developed in this study to better infer ancient global ocean redox conditions. A lack of overall correlation between δ^{98}Mo and δ^{238}U is observed from a compilation of coupled Mo-U isotope data from the same samples of euxinic post-Archean ORMs, indicating that both local depositional factors and global ocean redox states exert significant influence on the sedimentary Mo and U isotope compositions. Negative, positive, and no correlations are observed from the covariations of the coupled Mo-U isotope data in the individual euxinic ORM units. Hence, each euxinic ORM unit must be carefully evaluated on a case-by-case basis to disentangle changes in local depositional conditions from global ocean redox variations.

A negative correlation between the Mo and U isotope compositions, similar to the observations from modern euxinic basins, is observed for the Upper Devonian Kettle Point Formation. This negative correlation most likely reflects changes in local depositional conditions with a generally stable global ocean redox state that, in the case of the Late Devonian (Famennian), was only slightly less oxygenated than the modern oceans. A lack of correlation between the Mo-U isotope compositions for upper unit 4 of the Kettle Point Formation implies relatively constant bottom water sulfide concentrations. The Fe-Mn particulate shuttle could contribute to but is not the main cause of the low Mo isotope compositions.

A positive correlation between Mo and U isotope compositions points to a change in global ocean redox conditions during deposition of euxinic ORM. Such a

positive correlation is observed for the Upper Ordovician (Katian) Fjäcka Shale, suggesting a transient episode of increased ocean oxygenation that simultaneously shifted the euxinic sediment Mo and U isotope compositions to higher values. This interpretation supports previous studies that suggested dynamic ocean redox conditions occurred during the Early Paleozoic Era.

No correlations are observed in many ORM units, which may be related to relatively stable depositional environment at local and global scales, specific changes in the local depositional environment, a combination of changes in local depositional conditions and global ocean redox state, or may simply be an artifact of limited data.

The Tanezzuft Formation represents a case of relatively constant local depositional conditions and global ocean redox conditions. This interpretation is supported by no directional stratigraphic changes of various geochemical proxies and narrow ranges of Mo and U isotope compositions of the euxinic shales from this formation.

The Doushantuo Formation Member IV is an excellent example that shows the combined effects of local (e.g., Fe-Mn particulate shuttle, changing bottom water sulfide concentrations, bottom water renewal rates associated with basin restrictions) and global variations (e.g., changing ocean redox conditions). Detailed analyses of the geochemical data suggest widespread ocean oxygenation throughout much of Member IV time, whereas an expansion of ocean anoxia is inferred during uppermost Member IV time.

The Zaonega Formation represents potentially variable extents of basin restriction during deposition. The coupled Mo-U isotope data exhibits a generally horizontal trend that is similar to upper unit 4 of the Kettle Point Formation with only one sample that has a higher δ^{98}Mo value. This lone sample with a higher δ^{98}Mo might

be deposited during a transient period of strong basin restriction that caused sluggish bottom water ventilation and renewal, whereas the horizontal trend defined by the other samples suggests that relatively constant bottom water sulfide concentrations resulted in similar magnitudes of Mo isotope fractionations and several processes (e.g., U reduction pathways, efficiency of U reduction and removal, aqueous U species) caused variable U isotope fractionations.

For the ORMs with limited data, there are large uncertainties associated with inferring global seawater Mo and U isotope compositions. Nevertheless, the coupled high δ^{98}Mo (nearly similar to modern seawater) and high δ^{238}U of the Upper Devonian Chattanooga Shale and New Albany Shale represents strong evidence of widespread ocean oxygenation at that time.

Building upon recent studies of modern euxinic basins, our study highlights the potential of using coupled Mo-U isotope data from euxinic ORM units to disentangle the effects of the local depositional environment and global ocean redox states. Using this approach, we have revealed some features that were not identified in previous studies. We have also demonstrated how the contemporaneous global seawater Mo and U isotope compositions during euxinic ORM deposition can be estimated through a coupled Mo-U isotope mass balance model. Our study demonstrates the necessity of carefully determining the local depositional environment (e.g., basin restriction, bottom water redox conditions, operation of an Fe-Mn particulate shuttle) before interpreting global ocean redox tracers (e.g., δ^{98}Mo and δ^{238}U) and highlights the necessity of using large datasets of coupled Mo and U isotope data to better infer local and global ocean redox dynamics.

Acknowledgments

We thank Noah Planavsky and two anonymous reviewers for constructive comments that greatly improved this manuscript, and associate editor Claudine Stirling for editorial handling. We thank Liyan Xing for assistance with preparation of samples for U isotope analysis. Please contact Tais W. Dahl for samples that were analyzed for U isotope data in this study. This study was supported by a NSERC Discovery Grant (grant number RGPIN-2013-435930 and RGPIN-2019-0409) and an Ontario Early Researcher Award to BK, the Carlsberg Foundation (CF16-0876) and the Danish Council for Independent Research (DFF - 7014-00295, DFF-8102-00005B) to TWD, and a Student Research Grant from the Geological Society of America to XL. The Metal Isotope Geochemistry Laboratory at Waterloo was funded by the Canada Foundation for Innovation, Ontario Research Fund, and University of Waterloo.

References

Abe, M., Suzuki, T., Fujii, Y., Hada, M. and Hirao, K. (2008) An ab initio molecular orbital study of the nuclear volume effects in uranium isotope fractionations. *J. Chem. Phys.* **129,** 164309.

Algeo, T. J. (2004) Can marine anoxic events draw down the trace element inventory of seawater? *Geology* **32,** 1057-1060.

Algeo, T. J. and Lyons, T. W. (2006) Mo-total organic carbon covariation in modern anoxic marine environments: Implications for analysis of paleoredox and paleohydrographic conditions. *Paleoceanography* **21,** PA1016.

Algeo, T. J. and Tribovillard, N. (2009) Environmental analysis of paleoceanographic systems based on molybdenum–uranium covariation. *Chem. Geol.* **268,** 211-225.

Andersen, M. B., Elliott, T., Freymuth, H., Sims, K. W., Niu, Y. and Kelley, K. A. (2015) The terrestrial uranium isotope cycle. *Nature* **517,** 356-359.

Andersen, M. B., Matthews, A., Vance, D., Bar-Matthews, M., Archer, C. and de Souza, G. F. (2018) A 10-fold decline in the deep Eastern Mediterranean thermohaline overturning circulation during the last interglacial period. *Earth Planet. Sci. Lett.* **503,** 58-67.

Andersen, M. B., Romaniello, S., Vance, D., Little, S. H., Herdman, R. and Lyons, T. W. (2014) A modern framework for the interpretation of $^{238}U/^{235}U$ in studies of ancient ocean redox. *Earth Planet. Sci. Lett.* **400,** 184-194.

Andersen, M. B., Stirling, C. H. and Weyer, S. (2017) Uranium Isotope Fractionation. *Rev. Mineral. Geochem.* **82,** 799-850.

Andersen, M. B., Vance, D., Morford, J. L., Bura-Nakić, E., Breitenbach, S. F. M. and Och, L. (2016) Closing in on the marine $^{238}U/^{235}U$ budget. *Chem. Geol.* **420,** 11-22.

Anderson, R. F., Fleisher, M. Q. and Lehuray, A. P. (1989) Concentration, oxidation state, and particulate flux of uranium in the Black Sea. *Geochim. Cosmochim. Acta* **53,** 2215-2224.

Archer, C. and Vance, D. (2008) The isotopic signature of the global riverine molybdenum flux and anoxia in the ancient oceans. *Nat. Geosci.* **1,** 597-600.

Ardakani, O. H., Chappaz, A., Sanei, H. and Mayer, B. (2016) Effect of thermal maturity on remobilization of molybdenum in black shales. *Earth Planet. Sci. Lett.* **449,** 311-320.

Arnold, G. L., Anbar, A. D., Barling, J. and Lyons, T. W. (2004) Molybdenum isotope evidence for widespread anoxia in mid-Proterozoic oceans. *Science* **304,** 87-90.

Arnold, G. L., Lyons, T. W., Gordon, G. W. and Anbar, A. D. (2012) Extreme change

in sulfide concentrations in the Black Sea during the Little Ice Age reconstructed using molybdenum isotopes. *Geology* **40,** 595-598.

Asael, D., Rouxel, O., Poulton, S. W., Lyons, T. W. and Bekker, A. (2018) Molybdenum record from black shales indicates oscillating atmospheric oxygen levels in the early Paleoproterozoic. *Am. J. Sci.* **318,** 275-299.

Asael, D., Tissot, F. L. H., Reinhard, C. T., Rouxel, O., Dauphas, N., Lyons, T. W., Ponzevera, E., Liorzou, C. and Chéron, S. (2013) Coupled molybdenum, iron and uranium stable isotopes as oceanic paleoredox proxies during the Paleoproterozoic Shunga Event. *Chem. Geol.* **362,** 193-210.

Barling, J. and Anbar, A. D. (2004) Molybdenum isotope fractionation during adsorption by manganese oxides. *Earth Planet. Sci. Lett.* **217,** 315-329.

Barling, J., Arnold, G. L. and Anbar, A. D. (2001) Natural mass-dependent variations in the isotopic composition of molybdenum. *Earth Planet. Sci. Lett.* **193,** 447-457.

Barnes, C. E. and Cochran, J. K. (1990) Uranium removal in oceanic sediments and the oceanic U balance. *Earth Planet. Sci. Lett.* **97,** 94-101.

Barnes, C. E. and Cochran, J. K. (1993) Uranium geochemistry in estuarine sediments: Controls on removal and release processes. *Geochim. Cosmochim. Acta* **57,** 555-569.

Bartlett, R., Elrick, M., Wheeley, J. R., Polyak, V., Desrochers, A. and Asmerom, Y. (2018) Abrupt global-ocean anoxia during the Late Ordovician-early Silurian detected using uranium isotopes of marine carbonates. *Proc. Natl. Acad. Sci. U.S.A.* **115,** 5896-5901.

Basu, A., Sanford, R. A., Johnson, T. M., Lundstrom, C. C. and Löffler, F. E. (2014) Uranium isotopic fractionation factors during U(VI) reduction by bacterial

isolates. *Geochim. Cosmochim. Acta* **136,** 100-113.

Bekker, A. and Holland, H. D. (2012) Oxygen overshoot and recovery during the early Paleoproterozoic. *Earth Planet. Sci. Lett.* **317-318,** 295-304.

Bertine, K. K. and Turekian, K. K. (1973) MoIybdenum in marine deposits. *Geochim. Cosmochim. Acta* **37,** 1415-1434.

Bigeleisen, J. (1996) Nuclear Size and Shape Effects in Chemical Reactions. Isotope Chemistry of the Heavy Elements. *J. Am. Chem. Soc.* **118,** 3676-3680.

Bingham-Koslowski, N., Tsujita, C., Jin, J., Azmy, K. and Melchin, M. (2016) Widespread Late Devonian marine anoxia in eastern North America: a case study of the Kettle Point Formation black shale, southwestern Ontario. *Can. J. Earth Sci.* **53,** 837-855.

Brown, S. T., Basu, A., Ding, X., Christensen, J. N. and DePaolo, D. J. (2018) Uranium isotope fractionation by abiotic reductive precipitation. *Proc. Natl. Acad. Sci. U.S.A.* **115,** 8688-8693.

Brüske, A., Weyer, S., Zhao, M.-Y., Planavsky, N. J., Wegwerth, A., Neubert, N., Dellwig, O., Lau, K. V. and Lyons, T. W. (2020) Correlated molybdenum and uranium isotope signatures in modern anoxic sediments: implications for their use as paleo-redox proxy. *Geochim. Cosmochim. Acta* **270,** 449-474.

Bura-Nakić, E., Andersen, M. B., Archer, C., de Souza, G. F., Marguš, M. and Vance, D. (2018) Coupled Mo-U abundances and isotopes in a small marine euxinic basin: Constraints on processes in euxinic basins. *Geochim. Cosmochim. Acta* **222,** 212-229.

Butterfield, N. J. (2009) Oxygen, animals and oceanic ventilation: an alternative view. *Geobiology,* **7,** 1-7.

Canfield, D. E., Poulton, S. W. and Narbonne, G. M. (2007) Late-Neoproterozoic deep-

ocean oxygenation and the rise of animal life. *Science* **315,** 92-95.

Chen, X., Ling, H. F., Vance, D., Shields-Zhou, G. A., Zhu, M., Poulton, S. W., Och, L. M., Jiang, S. Y., Li, D., Cremonese, L. and Archer, C. (2015) Rise to modern levels of ocean oxygenation coincided with the Cambrian radiation of animals. *Nat. Commun.* **6,** 7142.

Chen, X., Romaniello, S. J. and Anbar, A. D. (2017) Uranium isotope fractionation induced by aqueous speciation: Implications for U isotopes in marine $CaCO_3$ as a paleoredox proxy. *Geochim. Cosmochim. Acta* **215,** 162-172.

Chen, X., Romaniello, S. J., Herrmann, A. D., Hardisty, D., Gill, B. C. and Anbar, A. D. (2018a) Diagenetic effects on uranium isotope fractionation in carbonate sediments from the Bahamas. *Geochim. Cosmochim. Acta* **237,** 294-311.

Chen, X., Romaniello, S. J., Herrmann, A. D., Samankassou, E. and Anbar, A. D. (2018b) Biological effects on uranium isotope fractionation ($^{238}U/^{235}U$) in primary biogenic carbonates. *Geochim. Cosmochim. Acta* **240,** 1-10.

Clark, S. K. and Johnson, T. M. (2008) Effective isotopic fractionation factors for solute removal by reactive sediments: A laboratory microcosm and slurry study. *Environ. Sci. Technol.* **42,** 7850-7855.

Cocks, L. R. M. and Torsvik, T. H. (2005) Baltica from the late Precambrian to mid-Palaeozoic times: The gain and loss of a terrane's identity. *Earth-Sci. Rev.* **72,** 39-66.

Cole, D. B., Planavsky, N. J., Longley, M., Böning, P., Wilkes, D., Wang, X., Swanner, E. D., Wittkop, C., Loydell, D., Busigny, V., Knudsen, A., Sperling, E. A. (2020) Uranium isotope fractionation in non-sulfidic anoxic settings and the global uranium isotope mass balance. *Global Biogeochem. Cycles.* doi: https://doi.org/10.1029/2020GB006649

Dahl, T. W., Canfield, D. E., Rosing, M. T., Frei, R. E., Gordon, G. W., Knoll, A. H. and Anbar, A. D. (2011) Molybdenum evidence for expansive sulfidic water masses in ~750Ma oceans. *Earth Planet. Sci. Lett.* **311,** 264-274.

Dahl, T. W., Chappaz, A., Fitts, J. P. and Lyons, T. W. (2013) Molybdenum reduction in a sulfidic lake: Evidence from X-ray absorption fine-structure spectroscopy and implications for the Mo paleoproxy. *Geochim. Cosmochim. Acta* **103,** 213-231.

Dahl, T. W., Chappaz, A., Hoek, J., McKenzie, C. J., Svane, S. and Canfield, D. E. (2017a) Evidence of molybdenum association with particulate organic matter under sulfidic conditions. *Geobiology* **15,** 311-323.

Dahl, T. W., Connelly, J. N., Kouchinsky, A., Gill, B. C., Månsson, S. F. and Bizzarro, M. (2017b) Reorganisation of Earth's biogeochemical cycles briefly oxygenated the oceans 520 Myr ago. *Geochem. Perspect. Lett.* **3,** 210-220.

Dahl, T. W., Connelly, J. N., Li, D., Kouchinsky, A., Gill, B. C., Porter, S., Maloof, A. C. and Bizzarro, M. (2019) Atmosphere-ocean oxygen and productivity dynamics during early animal radiations. *Proc. Natl. Acad. Sci. U. S. A.* **116,** 19352-19361.

Dahl, T. W. and Hammarlund, E. U. (2011) "Do large predatory fish track ocean oxygenation?" *Commun. Integr. Biol.* **4,** 92-94.

Dahl, T. W., Hammarlund, E. U., Anbar, A. D., Bond, D. P. G., Gill, B. C., Gordon, G. W., Knoll, A. H., Nielsen, A. T., Schovsbo, N. H. and Canfield, D. E. (2010) Devonian rise in atmospheric oxygen correlated to the radiations of terrestrial plants and large predatory fish. *Proc. Natl. Acad. Sci. U.S.A.* **107,** 17911-17915.

Davidson, L., Beswetherick, S., Craig, J., Eales, M., Fisher, A., Himmali, A., Jho, J., Mejrab, B., Smart, J., 2000. The structure, stratigraphy and petroleum geology

of the Murzuq Basin, southwest Libya. In *Geological Exploration in the Murzuq Basin* (eds. M. A. Sola and D. Worsley). Elsevier, Amsterdam, pp. 295-320.

Dellwig, O., Leipe, T., März, C., Glockzin, M., Pollehne, F., Schnetger, B., Yakushev, E. V., Böttcher, M. E. and Brumsack, H.-J. (2010) A new particulate Mn–Fe–P-shuttle at the redoxcline of anoxic basins. *Geochim. Cosmochim. Acta* **74,** 7100-7115.

Dellwig, O., Schnetger, B., Brumsack, H.-J., Grossart, H.-P. and Umlauf, L. (2012). Dissolved reactive manganese at pelagic redoxclines (part II): Hydrodynamic conditions for accumulation. *J. Mar. Sys.* **90,** 31-41.

Desio, A. (1936) Riassunto sulla presenza del Silurico fossilifero nel Fezzan. *Bollettino. Soc. Geol. Ital.* **55,** 319-356.

Diamond, C. W., Planavsky, N. J., Wang, C., & Lyons, T. W. (2018). What the ~1.4 Ga Xiamaling Formation can and cannot tell us about the mid-Proterozoic ocean. *Geobiology* **16,** 219-236.

Diaz, R. and Rosenberg, R. (1995) Marine benthic hypoxia: A review of its ecological effects and the behavioural response of benthic macrofauna. *Oceanogr. Mar. Biol. Ann. Rev.* **33,** 245-303.

Dickson, A. J., Idiz, E., Porcelli, D., & van den Boorn, S. H. J. M. (2019). The influence of thermal maturity on the stable isotope compositions and concentrations of molybdenum, zinc and cadmium in organic-rich marine mudrocks. *Geochim. Cosmochim. Acta.* doi: http://doi.org/10.1016/j.gca.2019.11.001

Dunk, R. M., Mills, R. A. and Jenkins, W. J. (2002) A reevaluation of the oceanic uranium budget for the Holocene. *Chem. Geol.* **190,** 45-67.

Emerson, S. R. and Huested, S. S. (1991) Ocean anoxia and the concentrations of molybdenum and vanadium in seawater. *Mar. Chem.* **34,** 177-196.

Endrizzi, F., Leggett, C. J. and Rao, L. (2016) Scientific Basis for Efficient Extraction of Uranium from Seawater. I: Understanding the Chemical Speciation of Uranium under Seawater Conditions. *Ind. Eng. Chem. Res.* **55,** 4249–4256.

Erickson, B. E. and Helz, G. R. (2000) Molybdenum(VI) speciation in sulfidic waters: Stability and lability of thiomolybdates. *Geochim. Cosmochim. Acta* **64,** 1149-1158.

Eroglu, S., Scholz, F., Frank, M. and Siebert, C. (2020) Influence of particulate versus diffusive molybdenum supply mechanisms on the molybdenum isotope composition of continental margin sediments. *Geochim. Cosmochim. Acta.* **273,** *51-69*

Farquhar, J., Bao, H. and Thiemens, M. (2000) Atmospheric influence of Earth's earliest sulfur cycle. *Science* **289,** 756–758.

Gilleaudeau, G. J., Romaniello, S. J., Luo, G., Kaufman, A. J., Zhang, F., Klaebe, R. M., Kah, L. C., Azmy, K., Bartley, J. K., Zheng, W., Knoll, A. H. and Anbar, A. D. (2019). Uranium isotope evidence for limited euxinia in mid-Proterozoic oceans. *Earth Planet. Sci. Lett.* **521,** 150-157.

Goldberg, T., Archer, C., Vance, D. and Poulton, S. W. (2009) Mo isotope fractionation during adsorption to Fe (oxyhydr)oxides. *Geochim. Cosmochim. Acta* **73,** 6502-6516.

Goldberg, T., Archer, C., Vance, D., Thamdrup, B., McAnena, A. and Poulton, S. W. (2012) Controls on Mo isotope fractionations in a Mn-rich anoxic marine sediment, Gullmar Fjord, Sweden. *Chem. Geol.* **296-297,** 73-82.

Goldberg, T., Poulton, S. W., Wagner, T., Kolonic, S. F. and Rehkämper, M. (2016) Molybdenum drawdown during Cretaceous Oceanic Anoxic Event 2. *Earth*

Planet. Sci. Lett. **440,** 81-91.

Gordon, G. W., Lyons, T. W., Arnold, G. L., Roe, J., Sageman, B. B. and Anbar, A. D. (2009) When do black shales tell molybdenum isotope tales? *Geology* **37,** 535-538.

Goto, K. T., Anbar, A. D., Gordon, G. W., Romaniello, S. J., Shimoda, G., Takaya, Y., Tokumaru, A., Nozaki, T., Suzuki, K., Machida, S., Hanyu, T. and Usui, A. (2014) Uranium isotope systematics of ferromanganese crusts in the Pacific Ocean: Implications for the marine $^{238}U/^{235}U$ isotope system. *Geochim. Cosmochim. Acta* **146,** 43-58.

Hamblin, A. P. (2010) Detailed outcrop and core measured sections of the Kettle Point formation, southwestern Ontario, with reference to shale gas potential. *Geological Survey of Canada*, Open File 6579, 26p.

Hammarlund, E. U., Dahl, T. W., Harper, D. A. T., Bond, D. P. G., Nielsen, A. T., Bjerrum, C. J., Schovsbo, N. H., Schönlaub, H. P., Zalasiewicz, J. A. and Canfield, D. E. (2012) A sulfidic driver for the end-Ordovician mass extinction. *Earth Planet. Sci. Lett.* **331-332,** 128-139.

Hannah, J. L., Stein, H. J., Zimmerman, A., Yang, G., Melezhik, V. A., Filippov, M. M., Turgeon S. C. and Creaser, R. A. (2008) Re-Os geochronology of shungite: a 2.05 Ga fossil oil field in Karelia. *Geochimica et Cosmochimica Acta* **72,** A351.

Hardisty, D. S., Lu, Z., Bekker, A., Diamond, C. W., Gill, B. C., Jiang, G., Kah, L. C., Knoll, A. H., Loyd, S. J., Osburn, M. R., Planavsky, N. J., Wang, C., Zhou, X. and Lyons, T. W. (2017) Perspectives on Proterozoic surface ocean redox from iodine contents in ancient and recent carbonate. *Earth Planet. Sci. Lett.* **463,** 159-170.

Helz, G. R., Bura-Nakić, E., Mikac, N. and Ciglenečki, I. (2011) New model for

molybdenum behavior in euxinic waters. *Chem. Geol.* **284,** 323-332.

Helz, G. R., Miller, C. V., Charnock, J. M., Mosselmans, J. F. W., Pattrick, R. A. D., Garner, C. D. and Vaughan, D. J. (1996) Mechanism of molybdenum removal from the sea and its concentration in black shales: EXAFS evidence. *Geochim. Cosmochim. Acta* **60,** 3631-3642.

Holland, H. D. (2006). The oxygenation of the atmosphere and oceans. *Philos. Trans. R. Soc. Lond. B. Biol. Sci.* **361,** 903-915.

Holmden, C., Amini, M. and Francois, R. (2015) Uranium isotope fractionation in Saanich Inlet: A modern analog study of a paleoredox tracer. *Geochim. Cosmochim. Acta* **153,** 202-215.

Huckriede, H. and Meischner, D. (1996) Origin and environment of manganese-rich sediments within black-shale basins. *Geochim. Cosmochim. Acta* **60,** 1399-1413.

Jiang, G., Shi, X., Zhang, S., Wang, Y. and Xiao, S. (2011) Stratigraphy and paleogeography of the Ediacaran Doushantuo Formation (ca. 635–551Ma) in South China. *Gondwana Res.* **19,** 831-849.

Jiang G., Sohl L. E. and Christie-Blick N. (2003) Neoproterozoic stratigraphic comparison of the Lesser Himalaya (India) and Yangtze block (South China): Paleogeographic implications. *Geology* **31,** 917**–**920.

Kendall, B., Creaser, R. A., Gordon, G. W. and Anbar, A. D. (2009) Re–Os and Mo isotope systematics of black shales from the Middle Proterozoic Velkerri and Wollogorang Formations, McArthur Basin, northern Australia. *Geochim. Cosmochim. Acta* **73,** 2534-2558.

Kendall, B., Dahl, T. W. and Anbar, A. D. (2017) The stable isotope geochemistry of molybdenum. *Rev. Mineral. Geochem.* **82,** 683-732.

Kendall, B., Komiya, T., Lyons, T. W., Bates, S. M., Gordon, G. W., Romaniello, S. J.,

Jiang, G., Creaser, R. A., Xiao, S., McFadden, K., Sawaki, Y., Tahata, M., Shu, D., Han, J., Li, Y., Chu, X. and Anbar, A. D. (2015) Uranium and molybdenum isotope evidence for an episode of widespread ocean oxygenation during the late Ediacaran Period. *Geochim. Cosmochim. Acta* **156,** 173-193.

Kendall, B., Wang, J., Zheng, W., Romaniello, S. J., Jeffrey Over, D., Bennett, Y., Xing, L., Kunert, A., Boyes, C. and Liu, J. (2020) Inverse correlation between the molybdenum and uranium isotope compositions of Upper Devonian black shales caused by changes in local depositional conditions rather than global ocean redox variations. *Geochim. Cosmochim. Acta.* doi: http://doi.org/10.1016/j.gca.2020.01.026

Kendall, B. S., Creaser, R. A., Ross, G. M. and Selby, D. (2004) Constraints on the timing of Marinoan "Snowball Earth" glaciation by ^{187}Re–^{187}Os dating of a Neoproterozoic, post-glacial black shale in Western Canada. *Earth Planet. Sci. Lett.* **222,** 729-740.

King, E. K. and Pett-Ridge, J. C. (2018) Reassessing the dissolved molybdenum isotopic composition of ocean inputs: The effect of chemical weathering and groundwater. *Geology* **46,** 955-958.

King, E. K., Thompson, A., Chadwick, O. A. and Pett-Ridge, J. C. (2016) Molybdenum sources and isotopic composition during early stages of pedogenesis along a basaltic climate transect. *Chem. Geol.* **445,** 54-67.

Ku, T. L., Knauss, K. G. and Mathieu, G. G. (1977) Uranium in open ocean: concentration and isotopic composition*. *Deep-sea Res.* **24,** 1005-1017.

Langmuir, D. (1978) Uranium solution-mineral equilibria at low temperatures with applications to sedimentary ore deposits. *Geochim. Cosmochim. Acta* **42,** 547-569.

Lau, K. V., Lyons, T. W. and Maher, K. (2020) Uranium reduction and isotopic fractionation in reducing sediments: Insights from reactive transport modeling. *Geochim. Cosmochim. Acta*. doi: https://doi.org/10.1016/j.gca.2020.01.021

Lu, W., Ridgwell, A., Thomas, E., Hardisty, D. S., Luo, G., Algeo, T. J., Saltzman, M. R., Gill, B. C., Shen, Y., Ling, H., Edwards, C. T., Whalen, M. T., Zhou, X., Gutchess, K. M., Jin, L., Rickaby, R. E. M., Jenkyns, H. C., Lyons, T. W., Lenton, T. M., Kump, L. R. and Lu, Z. (2018) Late inception of a resiliently oxygenated upper ocean. *Science* **361,** 174-177.

Lu, X., Kendall, B., Stein, H. J. and Hannah, J. L. (2017a) Temporal record of osmium concentrations and $^{187}Os/^{188}Os$ in organic-rich mudrocks: Implications for the osmium geochemical cycle and the use of osmium as a paleoceanographic tracer. *Geochim. Cosmochim. Acta* **216,** 221-241.

Lu, X., Kendall, B., Stein, H. J., Li, C., Hannah, J. L., Gordon, G. W. and Ebbestad, J. O. R. (2017b) Marine redox conditions during deposition of Late Ordovician and Early Silurian organic-rich mudrocks in the Siljan ring district, central Sweden. *Chem. Geol.* **457,** 75-94.

Lüning, S., Craig, J., Loydell, D. K., Štorch, P. and Fitches, B. (2000) Lower Silurian 'hot shales' in North Africa and Arabia: regional distribution and depositional model. *Earth Sci. Rev.* **49,** 121–200.

Lowenstein, T. K., Kendall, B. and Anbar, A. D. (2014) The Geologic History of Seawater. *Treatise on Geochemistry, 2nd Edition,* 569-622.

Lyons, T. W., Reinhard, C. T. and Planavsky, N. J. (2014) The rise of oxygen in Earth's early ocean and atmosphere. *Nature* **506,** 307-315.

Mänd, K., Lalonde, S. V., Robbins, L. J., Thoby, M., Paiste, K., Kreitsmann, T., Paiste, P., Reinhard, C. T., Romashkin, A. E., Planavsky, N. J., Kirsimäe, K., Lepland,

A. and Konhauser, K. O. (2020) Palaeoproterozoic oxygenated oceans following the Lomagundi–Jatuli Event. *Nat. Geosci.* **13**, 302-306.

McManus, J., Berelson, W. M., Severmann, S., Poulson, R. L., Hammond, D. E., Klinkhammer, G. P. and Holm, C. (2006) Molybdenum and uranium geochemistry in continental margin sediments: Paleoproxy potential. *Geochim. Cosmochim. Acta* **70,** 4643-4662.

McManus, J., Nägler, T. F., Siebert, C., Wheat, C. G. and Hammond, D. E. (2002) Oceanic molybdenum isotope fractionation: Diagenesis and hydrothermal ridge-flank alteration. *Geochem. Geophys. Geosyst.* **3,** 1078.

Melezhik, V. A., Fallick, A. E., Brasier, A. T. and Lepland, A. (2015) Carbonate deposition in the Palaeoproterozoic Onega basin from Fennoscandia: a spotlight on the transition from the Lomagundi-Jatuli to Shunga events. *Earth-Sci. Rev.* **147,** 65-98.

Melezhik, V. A., Fallick, A. E., Filippov, M. M. and Larsen, O. (1999) Karelian shungite-an indication of 2.0-Ga-old metamorphosed oil-shale and generation of petroleum: geology, lithology and geochemistry. *Earth-Sci. Rev.* **47,** 1-40.

Melchin, M. J., Mitchell, C. E., Holmden, C. and Storch, P. (2013) Environmental changes in the Late Ordovician-early Silurian: Review and new insights from black shales and nitrogen isotopes. *Geol. Soc. Am. Bull.* **125,** 1635-1670.

Miller, C. A., Peucker-Ehrenbrink, B., Walker, B. D. and Marcantonio, F. (2011) Re-assessing the surface cycling of molybdenum and rhenium. *Geochim. Cosmochim. Acta* **75,** 7146-7179.

Mills, D. B. and D. E. Canfield (2014) Oxygen and animal evolution: did a rise of atmospheric oxygen "trigger" the origin of animals? *Bioessays* **36,** 1145-1155.

Montoya-Pino, C. (2011). *Molybdenum and Uranium Isotope Signatures of Mesozoic*

Black Shales: Implications on the Spatial Dimension of Oceanic Anoxic Events.

Montoya-Pino, C., Weyer, S., Anbar, A. D., Pross, J., Oschmann, W., van de Schootbrugge, B. and Arz, H. W. (2010) Global enhancement of ocean anoxia during Oceanic Anoxic Event 2: A quantitative approach using U isotopes. *Geology* **38,** 315-318.

Moore, W.S. (1996) Large groundwater inputs to coastal waters revealed by ^{226}Ra enrichments. *Nature* **380,** 612–614.

Morford, J. L. and Emerson, S. (1999) The geochemistry of redox sensitive trace metals in sediments. *Geochim. Cosmochim. Acta* **63,** 1735-1750.

Mukherjee, I. and Large, R. R. (2016) Pyrite trace element chemistry of the Velkerri Formation, Roper Group, McArthur Basin: Evidence for atmospheric oxygenation during the Boring Billion. *Precambrian Res.* **281,** 13-26.

Nägler, T. F., Anbar, A. D., Archer, C., Goldberg, T., Gordon, G. W., Greber, N. D., Siebert, C., Sohrin, Y. and Vance, D. (2014) Proposal for an International Molybdenum Isotope Measurement Standard and Data Representation. *Geostand. Geoanal. Res.* **38,** 149-151.

Nägler, T. F., Neubert, N., Böttcher, M. E., Dellwig, O. and Schnetger, B. (2011) Molybdenum isotope fractionation in pelagic euxinia: Evidence from the modern Black and Baltic Seas. *Chem. Geol.* **289,** 1-11.

Nakagawa, Y., Takano, S., Firdaus, M. L., Norsuye, K., Hirata, T., Vance, D. and Sohrin, Y. (2012) The molybdenum isotopic composition of the modern ocean. *Geochim. Cosmochim. Acta* **46,** 131-141.

Neely, R. A., Gislason, S. R., Ólafsson, M., McCoy-West, A. J., Pearce, C. R. and Burton, K. W. (2018) Molybdenum isotope behaviour in groundwaters and terrestrial hydrothermal systems, Iceland. *Earth Planet. Sci. Lett.* **486,** 108-118.

Neubert, N., Nägler, T. F. and Böttcher, M. E. (2008) Sulfidity controls molybdenum isotope fractionation into euxinic sediments: Evidence from the modern Black Sea. *Geology* **36,** 775-778.

Noordmann, J., Weyer, S., Georg, R. B., Jons, S. and Sharma, M. (2016) $^{238}U/^{235}U$ isotope ratios of crustal material, rivers and products of hydrothermal alteration: new insights on the oceanic U isotope mass balance. *Isot. Environ. Health Stud.* **52,** 141-163.

Noordmann, J., Weyer, S., Montoya-Pino, C., Dellwig, O., Neubert, N., Eckert, S., Paetzel, M. and Böttcher, M. E. (2015) Uranium and molybdenum isotope systematics in modern euxinic basins: Case studies from the central Baltic Sea and the Kyllaren fjord (Norway). *Chem. Geol.* **396,** 182-195.

Ostrander, C. M., Sahoo, S. K., Kendall, B., Jiang, G., Planavsky, N. J., Lyons, T. W., Nielsen, S. G., Owens, J. D., Gordon, G. W., Romaniello, S. J. and Anbar, A. D. (2019a) Multiple negative molybdenum isotope excursions in the Doushantuo Formation (South China) fingerprint complex redox-related processes in the Ediacaran Nanhua Basin. *Geochim. Cosmochim. Acta* **261,** 191-209.

Ostrander, C. M., Nielsen, S. G., Owens, J. D., Kendall, B., Gordon, G. W., Romaniello, S. J. and Anbar, A. D. (2019b) Fully oxygenated water columns over continental shelves before the Great Oxidation Event. *Nat. Geosci.* **12,** 186-191.

Paiste, K., Lepland, A., Zerkle, A. L., Kirsimäe, K., Izon, G., Patel, N. K., McLean, F., Kreitsmann, T., Mänd, K., Bui, T. H., Romashkin, A. E., Rychanchik, D. V. and Prave, A. R. (2018) Multiple sulphur isotope records tracking basinal and global processes in the 1.98 Ga Zaonega Formation, NW Russia. *Chem. Geol.* **499,** 151-164.

Partin, C. A., Bekker, A., Planavsky, N. J., Scott, C. T., Gill, B. C., Li, C., Podkovyrov, V., Maslov, A., Konhauser, K. O., Lalonde, S. V., Love, G. D., Poulton, S. W. and Lyons, T. W. (2013) Large-scale fluctuations in Precambrian atmospheric and oceanic oxygen levels from the record of U in shales. *Earth Planet. Sci. Lett.* **369-370,** 284-293.

Pavlov, A. A. and Kasting, J. F. (2002) Mass-independent fractionation of sulfur isotopes in Archean sediments: strong evidence for an anoxic Archean atmosphere. *Astrobiology* **2,** 27-41.

Payne, J. L., McClain, C. R., Boyer, A. G., Brown, J. H., Finnegan, S., Kowalewski, M., Krause, R. A. Jr., Lyons, S. K., McShea, D. W., Novack-Gottshall, P. M., Smith, F. A., Spaeth, P., Stempien, J. A. and Wang, S. C. (2011) The evolutionary consequences of oxygenic photosynthesis: a body size perspective. *Photosynth. Res.* **107,** 37-57.

Planavsky, N. J., McGoldrick, P., Scott, C. T., Li, C., Reinhard, C. T., Kelly, A. E., Chu, X., Bekker, A., Love, G. D. and Lyons, T. W. (2011) Widespread iron-rich conditions in the mid-Proterozoic ocean. *Nature* **477,** 448-451.

Planavsky, N. J., Reinhard, C. T., Wang, X., Thomson, D., McGoldrick, P., Rainbird, R. H., Johnson, T., Fischer, W. W., and Lyons, T. W. (2014) Low Mid-Proterozoic atmospheric oxygen levels and the delayed rise of animals. *Science* **346,** 635-638.

Poulson Brucker, R. L., McManus, J., Severmann, S. and Berelson, W. M. (2009) Molybdenum behavior during early diagenesis. *Geochem. Geophys. Geosyst.* **10,** Q06010.

Poulson, R. L., Siebert, C., McManus, J. and Berelson, W. M. (2006) Authigenic molybdenum isotope signatures in marine sediments. *Geology* **34,** 617.

Poulton, S. W. and Canfield, D. E. (2005) Development of a sequential extraction procedure for iron: implications for iron partitioning in continentally derived particulates. *Chem. Geol.* **214,** 209-221.

Poulton, S. W. and Canfield, D. E. (2011) Ferruginous Conditions: A Dominant Feature of the Ocean through Earth's History. *Elements* **7,** 107-112.

Poulton, S. W. and Raiswell, R. (2002) The low-temperature geochemical cycle of iron: From continental fluxes to marine sediment deposition. *Am. J. Sci.* **302,** 774-805.

Qu, Y., Crne, A. E., Lepland, A. and van Zuilen, M. A. (2012) Methanotrophy in a Paleoproterozoic oil field ecosystem, Zaonega Formation, Karelia, Russia. *Geobiology* **10,** 467-478.

Raiswell, R., Hardisty, D. S., Lyons, T. W., Canfield, D. E., Owens, J. D., Planavsky, N. J., Poulton, S. W. and Reinhard, C. T. (2018) The iron paleoredox proxies: A guide to the pitfalls, problems and proper practice. *Am. J. Sci.* **318,** 491-526.

Reinhard, C. T., Planavsky, N. J., Robbins, L. J., Partin, C. A., Gill, B. C., Lalonde, S. V., Bekker, A., Konhauser, K. O. and Lyons, T. W. (2013) Proterozoic ocean redox and biogeochemical stasis. *Proc. Natl. Acad. Sci. U.S.A.* **110,** 5357-5362.

Rhoads, D. C. and Morse, J. W. (1971) Evolutionary and ecologic significance of oxygen-deficient marine basins. *Lethaia* **4,** 413-428.

Rolison, J. M., Stirling, C. H., Middag, R. and Rijkenberg, M. J. A. (2017) Uranium stable isotope fractionation in the Black Sea: Modern calibration of the $^{238}U/^{235}U$ paleo-redox proxy. *Geochim. Cosmochim. Acta* **203,** 69-88.

Romaniello, S. J., Herrmann, A. D. and Anbar, A. D. (2013) Uranium concentrations and $^{238}U/^{235}U$ isotope ratios in modern carbonates from the Bahamas: Assessing a novel paleoredox proxy. *Chem. Geol.* **362,** 305-316.

Rooney, A. D., Chew, D. M., & Selby, D. (2011). Re–Os geochronology of the Neoproterozoic–Cambrian Dalradian Supergroup of Scotland and Ireland: Implications for Neoproterozoic stratigraphy, glaciations and Re–Os systematics. *Precambrian Res.* **185,** 202-214.

Sageman, B. B. and Lyons, T. W. (2003). Geochemistry of fine-grained sediments and sedimentary rocks. *Treatise on geochemistry*, 115-158.

Schauble, E. A. (2007) Role of nuclear volume in driving equilibrium stable isotope fractionation of mercury, thallium, and other very heavy elements. *Geochim. Cosmochim. Acta* **71,** 2170-2189.

Scholz, F., Baum, M., Siebert, C., Eroglu, S., Dale, A. W., Naumann, M. and Sommer, S. (2018) Sedimentary molybdenum cycling in the aftermath of seawater inflow to the intermittently euxinic Gotland Deep, Central Baltic Sea. *Chem. Geol.* **491,** 27-38.

Scholz, F., McManus, J. and Sommer, S. (2013) The manganese and iron shuttle in a modern euxinic basin and implications for molybdenum cycling at euxinic ocean margins. *Chem. Geol.* **355,** 56-68.

Scott, C., Lyons, T. W., Bekker, A., Shen, Y., Poulton, S. W., Chu, X. and Anbar, A. D. (2008) Tracing the stepwise oxygenation of the Proterozoic ocean. *Nature* **452,** 456-459.

Scott, C., Wing, B. A., Bekker, A., Planavsky, N. J., Medvedev, P., Bates, S. M., Yun, M. and Lyons, T. W. (2014) Pyrite multiple-sulfur isotope evidence for rapid expansion and contraction of the early Paleoproterozoic seawater sulfate reservoir. *Earth Planet. Sci. Lett.* **389,** 95-104.

Sheen, A. I., Kendall, B., Reinhard, C. T., Creaser, R. A., Lyons, T. W., Bekker, A., Poulton, S. W. and Anbar, A. D. (2018) A model for the oceanic mass balance

of rhenium and implications for the extent of Proterozoic ocean anoxia. *Geochim. Cosmochim. Acta* **227,** 75-95.

Siebert, C., McManus, J., Bice, A., Poulson, R. L. and Berelson, W. M. (2006) Molybdenum isotope signatures in continental margin marine sediments. *Earth Planet. Sci. Lett.* **241,** 723-733.

Siebert, C., Nägler, T. F., von Blanckenburg, F. and Kramers, J. D. (2003) Molybdenum isotope records as a potential new proxy for paleoceanography. *Earth Planet. Sci. Lett.* **211,** 159-171.

Sperling, E. A., Frieder, C. A., Raman, A. V., Girguis, P. R., Levin, L. A. and Knoll, A. H. (2013) Oxygen, ecology, and the Cambrian radiation of animals. *Proc. Natl. Acad. Sci. U.S.A.* **110,** 13446-13451.

Sperling, E. A., Wolock, C. J., Morgan, A. S., Gill, B. C., Kunzmann, M., Halverson, G. P., Macdonald, F. A., Knoll, A. H. and Johnston, D. T. (2015) Statistical analysis of iron geochemical data suggests limited late Proterozoic oxygenation. *Nature* **523,** 451-454.

Stirling, C. H., Andersen, M. B., Potter, E. and Halliday, A. N. (2007) Low-temperature isotopic fractionation of uranium. *Earth Planet. Sci. Lett.* **264,** 208-225.

Stirling, C. H., Andersen, M. B., Warthmann, R. and Halliday, A. N. (2015) Isotope fractionation of ^{238}U and ^{235}U during biologically-mediated uranium reduction. *Geochim. Cosmochim. Acta* **163,** 200-218.

Stockey, R. G., Cole, D. B., Planavsky, N. J., Loydell, D. K., Fryda, J. and Sperling, E. A. (2020) Persistent global marine euxinia in the early Silurian. *Nat. Commun.* **11,** 1804.

Stylo, M., Neubert, N., Wang, Y., Monga, N., Romaniello, S. J., Weyer, S. and Bernier-Latmani, R. (2015) Uranium isotopes fingerprint biotic reduction. *Proc. Natl.*

Acad. Sci. U.S.A. **112,** 5619-5624.

Tissot, F. L. H., Chen, C., Go, B. M., Naziemiec, M., Healy, G., Bekker, A., Swart, P. K. and Dauphas, N. (2018) Controls of eustasy and diagenesis on the $^{238}U/^{235}U$ of carbonates and evolution of the seawater ($^{234}U/^{238}U$) during the last 1.4 Myr. *Geochim. Cosmochim. Acta* **242,** 233-265.

Tissot, F. L. H. and Dauphas, N. (2015) Uranium isotopic compositions of the crust and ocean: Age corrections, U budget and global extent of modern anoxia. *Geochim. Cosmochim. Acta* **167,** 113-143.

Tostevin, R., Clarkson, M. O., Gangl, S., Shields, G. A., Wood, R. A., Bowyer, F., Penny, A. M., Stirling, C. H. and Stirling, C. H. (2019) Uranium isotope evidence for an expansion of anoxia in terminal Ediacaran oceans. *Earth Planet. Sci. Lett.* **506,** 104-112.

Voegelin, A. R., Pettke, T., Greber, N. D., von Niederhäusern, B. and Nägler, T. F. (2014) Magma differentiation fractionates Mo isotope ratios: Evidence from the Kos Plateau Tuff (Aegean Arc). *Lithos* **190-191,** 440-448.

Wallace, M. W., Hood, A. v. S., Shuster, A., Greig, A., Planavsky, N. J. and Reed, C. P. (2017) Oxygenation history of the Neoproterozoic to early Phanerozoic and the rise of land plants. *Earth Planet. Sci. Lett.* **466,** 12-19.

Wang, H., Zhang, Z., Li, C., Algeo, T. J., Cheng, M. and Wang, W. (2020) Spatiotemporal redox heterogeneity and transient marine shelf oxygenation in the Mesoproterozoic ocean. *Geochim. Cosmochim. Acta* **270,** 201-217.

Wang, X., Planavsky, N. J., Hofmann, A., Saupe, E. E., De Corte, B. P., Philippot, P., LaLonde, S. V., Jemison, N. E., Zou, H., Ossa, F. O., Rybacki, K., Alfimova, N., Larson, M. J., Tsikos, H., Fralick, P. W., Johnson, T. M., Knuden, A. C., Reinhard, C. T. and Konhauser, K. O. (2018) A Mesoarchean shift in uranium

isotope systematics. *Geochim. Cosmochim. Acta* **238,** 438-452.

Wang, X., Planavsky, N. J., Reinhard, C. T., Hein, J. R. and Johnson, T. M. (2016) A Cenozoic seawater redox record derived from $^{238}U/^{235}U$ in ferromanganese crusts. *Am. J. Sci.* **316,** 64-83.

Wang J. and Li Z.-X. (2003) History of Neoproterozoic rift basins in South China: implications for Rodinia breakup. *Precambrian Res.* **261,** 303–320.

Wasylenki, L. E., Rolfe, B. A., Weeks, C. L., Spiro, T. G. and Anbar, A. D. (2008) Experimental investigation of the effects of temperature and ionic strength on Mo isotope fractionation during adsorption to manganese oxides. *Geochim. Cosmochim. Acta* **72,** 5997-6005.

Wei, G.Y., Planavsky, N. J., Tarhan, L. G., Chen, X., Wei, W., Li, D. and Ling, H.-F. (2018) Marine redox fluctuation as a potential trigger for the Cambrian explosion. *Geology* **46,** 587-590.

Weyer, S., Anbar, A. D., Gerdes, A., Gordon, G. W., Algeo, T. J. and Boyle, E. A. (2008) Natural fractionation of $^{238}U/^{235}U$. *Geochim. Cosmochim. Acta* **72,** 345-359.

Willbold, M. and Elliott, T. (2017) Molybdenum isotope variations in magmatic rocks. *Chem. Geol.* **449,** 253-268.

Yang, S., Kendall, B., Lu, X., Zhang, F. and Zheng, W. (2017) Uranium isotope compositions of mid-Proterozoic black shales: Evidence for an episode of increased ocean oxygenation at 1.36 Ga and evaluation of the effect of post-depositional hydrothermal fluid flow. *Precambr. Res.* **298,** 187-201.

Zhang, S., Wang, X., Wang, H., Bjerrum, C. J., Hammarlund, E. U., Costa, M. M., Connelly, J. N., Zhang, B., Su, J. and Canfield, D. E. (2016) Sufficient oxygen for animal respiration 1,400 million years ago. *Proc. Natl. Acad. Sci. U.S.A.*

113, 1731-1736.

Zhang, F., Xiao, S., Kendall, B., Romaniello, S. J., Cui, H., Meyer, M., Gilleaudeau, G. J., Kaufman, A. J. and Anbar, A. D. (2018) Extensive marine anoxia during the terminal Ediacaran Period. *Sci. Adv.* **4,** eaan8983.

Zhang, F., Xiao, S., Romaniello, S. J., Hardisty, D., Li, C., Melezhik, V., Pokrovsky, B., Cheng, M., Shi, W., Lenton, T. M. and Anbar, A. D. (2019) Global marine redox changes drove the rise and fall of the Ediacara biota. *Geobiology* **17,** 594-610.

Zou, C., Qiu, Z., Poulton, S. W., Dong, D., Wang, H., Chen, D., Lu, B., Shi, Z., and Tao, H. (2018) Ocean euxinia and climate change "double whammy" drove the Late Ordovician mass extinction. *Geology* **46,** 535-538.

Tables

Table 1. Geochemical data for the euxinic ORM samples from eight formations in this study

Sample [a]	Depth (m)	TOC [b] (wt.%)	Al (wt.%)	Mo (μg/g)	Mo EF [e]	U (μg/g)	U EF [e]	$\delta^{98}Mo$ [c] (‰)	$\delta^{98}Mo_{auth}$ [e] (‰)	2SD measured	n [f]	$\delta^{238}U$ [d] (‰)	$\delta^{238}U_{auth}$ [e] (‰)	2SD measured	n [f]	Fe_{HR}/Fe_T	Fe_{py}/Fe_{HR}
New Albany & Chattanooga Shale, outcrop, USA 365 Ma																	
Clegg 873-B8+22		12.3	6.5	200.1	308.5	57.8	28.7	1.58	1.58	0.18	3	-0.14	-0.13	0.12	3	0.68	0.78
Chattanoga K8/7/94-22		13.6	5.6	236.5	425.0	76.5	44.3	1.65	1.66	0.10	3	-0.01	0.00	0.03	3	0.71	0.80
Chattanoga K8/7/94-23		14.7	5.3	257.9	489.9	81.7	50.1	1.85	1.85	0.13	2	0.00	0.01	0.09	3	0.66	0.70
Birkhill Shale, Dobs Linn outcrop, Scotland 442 Ma																	
DL6	13.3	1.4	6.0	17.7	29.7	8.2	4.4	1.36	1.40	0.17	3	-0.11	-0.06	0.11	3	0.44	0.73
Rastrites Shale, Billegrav-1 core, Sweden 442 Ma																	
BG-4	26.55	2.0	8.4	15.4	18.3	6.7	2.6	0.50	0.51	0.36	3	-0.09	0.05	0.08	3	0.45	0.78
Rastrites Shale, Lönstorp-1 core, Sweden 442 Ma																	
Lön97154	64.9	3.8	8.3	17.8	21.3	8.2	3.2	0.41	0.42	0.08	2	0.01	0.16	0.01	3	0.52	0.74
Lön97154 rep[g]	64.9		8.9	18.0	20.4	7.7	2.8					0.04	0.22	0.07	3		
Lön79002	72.4	1.0	7.8	5.6	7.2	4.3	1.8	0.69	0.75	0.23	2	-0.15		0.01	3	0.42	0.72
Almelund Shale, Albjära-1 core, Sweden 465 Ma																	
Alb79013	50.1	2.1	8.7	5.4	6.3	7.2	2.7	0.85	0.96	0.33	4	-0.29	-0.29	0.04	3	0.36	0.73
Alb79016	94.9	1.9	9.0	4.4	4.9	6.0	2.2	0.58	0.66	0.26	3	-0.29	-0.29	0.03	3	0.90	0.71
Alum Shale Formation, Albjära-1 core, Sweden 485 Ma																	
Alb97160	139.03	4.6	7.8	37.8	48.3	98.9	40.7	1.04	1.05	0.19	3	0.15	0.17	0.12	3	0.93	0.73
Alum Shale Formation, Gislövhammar-2 core, Sweden 485 Ma																	
Gis89934	24.03	7.3	7.6	69.4	91.7	45.9	19.6	0.46	0.46		1	0.06	0.08	0.01	3	0.44	0.71
Gis89933	26	8.7	7.7	132.1	170.9	44.4	18.5									0.55	0.74
Gis89933 rep[g]	26		7.9	136.8	173.5	44.8	18.3	0.20	0.20		1	0.16	0.19	0.04	3		

Gis89931	28	7.3	8.3	119.9	143.7	37.6	14.5	0.33	0.33	0.33	3	0.13	0.16	0.05	3	0.54	0.70
Alum Shale Formation, Andrarum-3 core, Sweden 500 Ma																	
Alum0760	7.6	12.4	7.5	111.1	148.4	132.2	57.0	1.07	1.07	0.09	3	-0.15	-0.14	0.07	3	1.25	0.78
Alum1178	11.78	7.1	7.4	51.2	69.1	28.5	12.4	0.93	0.94	0.17	2	0.03	0.05	0.06	3	1.35	0.75
Alum1200	12	9.1	7.4	60.1	80.8	33.3	14.5	0.97	0.98	0.10	2	0.02	0.04	0.13	4	1.35	0.80
Alum1300	13	9.1	7.3	44.6	61.2	20.6	9.1	1.23	1.24	0.06	2	-0.02	0.02	0.05	3	1.22	0.73
Alum1370	13.7	7.5	7.1	53.4	75.8	18.7	8.6	1.29	1.30	0.06	3	-0.04	-0.01	0.04	3	1.31	0.74
Yu'anshan Formation, Ma'fang core, China, 520 Ma																	
Cheng485	48.5	1.5	7.1	18.6	26.3	14.5	6.6	0.46	0.46	0.34	3	-0.03	0.02	0.08	3	0.51	0.85
Cheng476	47.6	1.3	7.2	7.6	10.6	8.8	4.0	0.51	0.53	0.17	4	-0.05	0.03	0.12	3	0.44	0.89
Cheng456	45.6	1.5	7.2	7.8	10.8	6.8	3.0	0.94	1.01	0.24	4	-0.19	-0.13	0.10	3	0.41	0.83
Cheng442	44.2	2.3	7.1	19.9	28.0	10.9	5.0	0.99	1.01	0.18	5	-0.08	-0.02	0.07	3	0.55	0.89
Cheng438	43.8	2.0	7.0	16.2	23.2	10.8	5.0	1.01	1.04	0.17	3	-0.04	0.02	0.05	3	0.50	0.85
Black River Dolomite, Forest-1 core, Tasmania, 640 Ma																	
RC06-FOR02-B	828.11-828.15	6.5	7.8	31.5	40.5	7.5	3.1	0.53	0.54	0.10	3	-0.05	0.07	0.03	3	0.79	0.93
RC06-FOR02-B rep[g]	828.11-828.15		6.6	26.4	40.2	6.6	3.2					-0.10	-0.01	0.07	3		
RC06-FOR02-D	828.23-828.27	6.6	11.3	43.5	38.5	11.7	3.3	0.55	0.56	0.18	6	-0.07	0.03	0.07	3	0.80	0.93
RC06-FOR02-G	828.37-828.40	6.5	7.1	29.3	41.2	6.9	3.1	0.46	0.46	0.21	6	-0.07	0.04	0.09	3	0.80	0.93
RC06-FOR02-H	828.48-828.50	6.4	6.8	28.6	41.8	6.9	3.2	0.39	0.39	0.10	3	-0.08	0.02	0.03	3	0.90	0.93
RC06-FOR02-H rep[g]	828.48-828.50		6.9	28.9	41.8	7.1	3.3					-0.10	-0.02	0.03	3		
RC06-FOR02-I	828.55 - 828.58	6.8	7.5	27.5	36.6	8.0	3.4	0.54	0.55	0.12	4	-0.13	-0.07	0.07	3	0.81	0.90

[a] Sample depth, Mo isotope data, TOC, and Fe speciation data are from Dahl et al. (2010)

[b] TOC = total organic carbon

[c] Mo isotope data reported relative to NIST SRM 3134 = 0.25‰

[d] U isotope data reported relative to CRM 145

[e] See calculation methods in section 3 of the main text

[f] Number of replicate analyses of the same sample solution

[g] rep = replicate samples

Table 2. Parameters used in the Mo and U isotope mass balance models for the modern seawater (see main text for references)

Parameters for the Mo isotope mass balance model		Parameters for the U isotope mass balance model	
δ_{input}	0.5 ± 0.2‰	δ_{input}	−0.29 ± 0.03‰
Δ^{a}_{EUX-SW}	−0.5 ± 0.3‰	Δ_{EUX-SW}	0.60 ± 0.20‰
Δ_{SAD-SW}	−0.9 ± 0.2‰	$\Delta_{OTHER-SW}$	0.05 ± 0.09‰
Δ_{OX-SW}	−3.0 ± 0.1‰	--	--
$f^{b}_{Mo\_EUX}$	5 ± 3%	f_{U_EUX}	9 ± 6%
f_{Mo_SAD}	50 ± 10%	f_{U_OTHER}	91 ± 6%
f_{Mo_OX}	45 ±10%	--	--
Modeled $\delta^{98}Mo_{SW}$	2.33 ± 0.24‰	Modeled $\delta^{238}U_{SW}$	−0.39 ± 0.10‰
Measured $\delta^{98}Mo_{SW}$	2.34 ± 0.10‰	Measured $\delta^{238}U_{SW}$	−0.39 ± 0.04‰

[a] Δ = the net Mo and U isotopic offsets between each sink and seawater

[b] f = the fractions of Mo and U removal into each sink

Table 3. Fractions of U burial and corresponding isotope fractionations of each U sink in the modern seawater.

Sinks		Fraction of U burial flux into each sink (%)	Fractionation factors [$\Delta_{sink\text{-}SW}$ (‰)]	References
Euxinic		9 ± 6	0.60 ± 0.20	1-6
Other reducing (Ferruginous sediments*)		40 ± 10	0.15 ± 0.16	1,3,6-11
Bio-carbonate		30 ± 10	0.01 ± 0.13	1,3,7,12,13
Hydrothermal alteration of crust	High-T	3 ± 3	0.00 ± 0.02	1,14-17
	Low-T	6 ± 6	0.25 ± 0.02	1,14-17
Oxic sediments		12 ± 6	−0.25	1,6,15-18
Weighted average of OTHER sink			0.05 ± 0.09%	

References: 1. Dunk et al. (2002); 2. Andersen et al. (2014); 3. Andersen et al. (2017); 4. Holmden et al. (2015); 5. Bura-Nakić et al. (2018); 6. Weyer et al. (2008); 7. Romaniello et al. (2013); 8. Andersen et al. (2016); 9. Chen et al. (2018a); 10. Tissot et al. (2018); 11. Noordmann et al. (2016); 12. Partin et al. (2013); 13. Chen et al. (2018b); 14. Andersen et al. (2015); 15. Barnes and Cochran (1990); 16. Morford and Emerson (1999); 17. Tissot and Dauphas (2015); 18. Cole et al. (2020);

* Ferruginous setting is not well understood.

Table 4. A summary of estimated ranges of global seawater Mo and U isotope compositions based on the coupled Mo-U isotope compositions of euxinic ORMs

Time (Ma)	ORM interval	Estimated δ^{98}Mo of coeval seawater	Estimated δ^{238}U of coeval seawater
2050	Zaonega Formation[1]	Scenario 1: 1.40‰ Scenario 2: 1.57‰ to 2.37‰	Scenario 1: −0.66‰ to −0.34‰ Scenario 2: −0.68‰ to −0.34‰
1360	upper Velkerri Formation[2, 3]	1.50‰ to 2.23‰	−0.70‰ to −0.34‰
640	Black River Dolomite[4]	1.45‰ to 1.75‰;	−0.78‰ to −0.55‰
555	Doushantuo Formation Member IV[4]	2.01‰ to 3.10‰ (Group 1 and 2); 1.32‰ to 1.60‰ (Group 3)	−0.64‰ to −0.34‰ (Group 1 and 2); −0.78‰ to −0.61‰ (Group 3)
520	Yu'anshan Formation[5, 6]	1.43‰ to 2.10‰	−0.77‰ to −0.34‰
500	Alum Shale[5, 6]	1.37‰ to 2.25‰	−0.72‰ to −0.34‰
485	Alum Shale[5, 6]	1.37‰ to 2.27‰	−0.78‰ to −0.34‰
465	Almelund Shale[5, 6, #]	N/A	N/A
448	Fjäcka Shale[7]	1.31‰ to 1.75‰ (early and late stage); 1.48‰ to 2.37‰ and, (middle stage)	−0.80‰ to −0.54‰, (early and late stage); −0.69‰ to −0.34‰ (middle stage)
442	Rastrite Shale[5, 6] and Birkhill Shale[5, 6, *]	1.37‰ to 2.27‰	−0.75‰ to −0.34‰

442	Tanezzuft Formation[9]	1.32‰ to 1.95‰	−0.78‰ to −0.34‰
372	Kettle Point Formation[8]	2.04‰ to 2.75‰ and	−0.61‰ to −0.34‰
365	Chattanooga Shale[5, 6] and New Albany Shale[5, 6, *]	1.82‰ to 2.25‰	−0.63‰ to −0.34‰

References: [1] Asael et al. (2013); [2] Kendall et al. (2009); [3] Yang et al. (2017); [4] Kendall et al. (2015); [5] Dahl et al. (2010); [6] This study;[7] Lu et al. (2017b); [8] Kendall et al. (2020); [9] Stockey et al., (2020).

[#] For the Almelund Shale, the coeval global seawater Mo and U isotope compositions are not estimated due to limited samples (n = 2).

*Because there is only one sample for the Birkhill Shale and New Albany Shale, the shales that were broadly co-deposited are used together to estimate the coeval seawater Mo and U isotope compositions.

Figure Captions

Figure 1. Covariations of Mo and U isotope compositions of sediments from modern euxinic basins (modified from Bura-Nakić et al., 2018). Circled points represent the averaged δ^{98}Mo-δ^{238}U of the euxinic basins (modified from Bura-Nakić et al. 2018 and see references therein). Other sources: Black Sea Unit I (Barling et al., 2001; Weyer et al., 2008; Arnold et al., 2012), Landsort Deep (Noordmann et al., 2015).

Figure 2. Covariations of the Mo and U isotope compositions of the euxinic organic-rich mudrocks from this study and previous publications. Horizontal and vertical dashed lines represent average upper crustal δ^{98}Mo (0.3‰; Voegelin et al., 2014; Willbold and Elliott, 2017) and δ^{238}U (−0.3‰; Andersen et al., 2015; Tissot and

Dauphas, 2015), respectively. See Table 1 and Table A1 for references.

Figure 3. a) The modeled seawater (SW) Mo and U isotope compositions under different redox conditions from a coupled Mo-U isotope mass balance model (see Section 5.1.1). The points on the same vertical black dashed lines have the same euxinic U burial fractions. The euxinic U burial fraction is 100% for the leftmost sample (f_{U_EUX} = f_{Mo_EUX} = 1) and decreases by 10% for each point towards its right (i.e. 90%, 80%, 70%, etc.). The curved colorful lines connect points that have the same SAD Mo burial fractions. The SAD Mo burial fraction is 100% for the lower right sample (f_{Mo_SAD} = 1, f_{U_EUX} = 0) and decreases by 10% for each line radiating outwards (i.e., 90%, 80%, 70%, etc.). b) Estimated potential ranges of modern seawater Mo and U isotope compositions (highlighted blue line) using samples deposited in modern euxinic basins (except the severely restricted Black Sea). Unrealistic solutions (e.g., EUX > SAD for Mo removal) of modern seawater are excluded. Data points of sediments are the averaged authigenic δ^{98}Mo and δ^{238}U for modern euxinic basins (see Figure 1 and references therein). Solid curve is from Bura-Nakić et al. (2018) and has a Δ^{98}Mo : Δ^{238}U ≈ −3 : 2, Δ^{98}Mo ≈ 0.9‰, and Δ^{238}U ≈ 0.6‰. The dotted and dashed curves have the same Δ^{98}Mo : Δ^{238}U ratios (−3 : 2) but Δ^{98}Mo = 1.8‰ and Δ^{238}U = 1.2‰, covering possible seawater-sediment U isotopic offsets up to the intrinsic U isotope fractionation factor of 1.2‰ associated with U^{6+} reduction. c) Estimated potential ranges of modern seawater Mo and U isotope compositions (highlighted blue line) using samples deposited under strong basin restrictions (the Black Sea). Unrealistic solutions (e.g., EUX > SAD for Mo removal) are excluded. The solid curves move horizontally to estimate the modern seawater isotope compositions (see Section 5.1.2 for details).

Figure 4. Illustration of the reconstruction of ancient seawater Mo and U isotope compositions based on coupled Mo-U isotope data of euxinic ORMs assuming deposition under a) non- or weakly-restricted basins and b) strongly-restricted basins. Yellow area represents the model solutions of seawater Mo and U isotope compositions and blue area represents the estimated seawater Mo and U isotope compositions using the proposed approach (see Section 5.1.3 for details). The curves (1, 2, 3 in a and 1', 2' in b) have the same $\Delta^{98}Mo : \Delta^{238}U$ ratios (−3 : 2) and $\Delta^{98}Mo$ = 1.8‰ and $\Delta^{238}U$ = 1.2‰.

Figure 5. Geochemical data of the Devonian Kettle Point Formation showing a) Mo vs TOC, b) Mo EF vs U EF, and c) $\delta^{98}Mo$ vs $\delta^{238}U$ (Table A1; Kendall et al., 2020). Dashed lines in a) represent regression slopes for four modern basins from Algeo and Lyons (2006) (Black Sea: 4.5 ± 1; Framvaren Fjord: 9 ± 2; Cariaco Basin: 25 ± 5; Saanich Inlet: 45 ± 5; in μg/g/wt.%). Dashed lines in b) represent the Mo/U ratios of modern seawater (1 × SW; Algeo and Tribovillard, 2009), and fractions of modern seawater (0.3 × SW and 3 × SW). The covariations of Mo and U enrichments and controlling mechanisms in b) are plotted following Algeo and Tribovillard (2009). Shaded area in c) represents the estimated ranges of coeval seawater Mo and U isotope compositions. Authigenic $\delta^{98}Mo$ and $\delta^{238}U$ data of euxinic samples are used. The dashed and dotted lines represent a Mo isotopic offset of −0.8‰ and −0.2‰ between the euxinic sink and seawater, respectively, by keeping all other parameters unchanged. This approach is applied to the following figures (Fig. 6-10).

Figure 6. Geochemical data of the Ordovician Fjäcka Shale showing a) Mo vs TOC, b) Mo EF vs U EF, and c) $\delta^{98}Mo$ vs $\delta^{238}U$ (Table A1; Lu et al., 2017b). The dotted and solid lines in c) are used to estimate ancient seawater isotope compositions for

stratigraphically middle samples and stratigraphically higher & lower samples, respectively.

Figure 7. Geochemical data of the Silurian Tanezzuft Formation showing a) Mo vs TOC, b) Mo EF vs U EF, and c) δ^{98}Mo vs δ^{238}U (Table A1; Stockey et al., 2020).

Figure 8. Geochemical data of the Paleoproterozoic Zaonega Formation showing a) Mo vs TOC, b) Mo EF vs U EF, and c) δ^{98}Mo vs δ^{238}U using euxinic samples only (Table A1; Asael et al., 2013). The dotted and solid lines in c) are used to estimate ancient seawater isotope compositions for an open marine environment and local basin restriction, respectively.

Figure 9. Geochemical data of the Ediacaran Doushantuo Formation Member IV showing a) Mo vs TOC, b) Mo EF vs U EF, and c) δ^{98}Mo vs δ^{238}U (group 1 and 2), and d) δ^{98}Mo vs δ^{238}U (group 3) (Table A1; Kendall et al., 2015). The vertical jump revealed between group 1 and 2 likely reflects that group 1 was significantly affected by a particulate Fe-Mn oxide shuttle.

Figure 10. Geochemical data of the rest of the ORM units that have no correlations between Mo and U isotope compositions. Plots of (a) Mo vs TOC, (b) Mo EF vs U EF, and (c) δ^{98}Mo vs δ^{238}U are shown for each of these ORM units (Table A1; Kendall et al., 2009, 2015; Dahl et al., 2010; Yang et al., 2017; Sheen et al., 2018; This study).

Declaration of interests

☒ The authors declare that they have no known competing financial interests or personal relationships that could have appeared to influence the work reported in this paper.

☐The authors declare the following financial interests/personal relationships which may be considered as potential competing interests: